



HAL
open science

The Lower in Vivo Osteogenicity of Adipose Tissue-Derived Stem Cells Correlates with a Higher Innate Immune Response

Manon Maroquenne, Marianne Bourguignon, Nathanael Larochette, Hanane El-Hafci, Morgane Margottin, Esther Potier, Delphine Logeart-Avramoglou

► **To cite this version:**

Manon Maroquenne, Marianne Bourguignon, Nathanael Larochette, Hanane El-Hafci, Morgane Margottin, et al.. The Lower in Vivo Osteogenicity of Adipose Tissue-Derived Stem Cells Correlates with a Higher Innate Immune Response. *Stem Cell Reviews and Reports*, 2023, 19 (8), pp.2869-2885. 10.1007/s12015-023-10614-1 . hal-04297756

HAL Id: hal-04297756

<https://hal.science/hal-04297756v1>

Submitted on 21 Nov 2023

HAL is a multi-disciplinary open access archive for the deposit and dissemination of scientific research documents, whether they are published or not. The documents may come from teaching and research institutions in France or abroad, or from public or private research centers.

L'archive ouverte pluridisciplinaire **HAL**, est destinée au dépôt et à la diffusion de documents scientifiques de niveau recherche, publiés ou non, émanant des établissements d'enseignement et de recherche français ou étrangers, des laboratoires publics ou privés.



Distributed under a Creative Commons Attribution - NonCommercial 4.0 International License

The lower in vivo osteogenicity of adipose tissue-derived stem cells correlates with a higher innate immune response

Authors : Manon Maroquenne^{1#}, Marianne Bourguignon^{1#}, Nathanael Larochette^{1#}, Hanane El-Hafci¹, Morgane Margottin¹, Esther Potier¹ and Delphine Logeart Avramoglou¹²

Co-first authors

Affiliations:

1: University Paris Cité, CNRS, INSERM, ENVA, Paris B3OA, F-75010, France

2: Laboratory of Bioengineering and Bioimaging for Osteo-Articular tissues UMR 7052 CNRS, Univ Paris Cité, 10 Avenue de Verdun, Paris F-75010, France

Key words: Adipose tissue stem cells • Bone marrow mesenchymal stem cells • Bone • Tissue regeneration • innate immune response

Abstract: Adipose tissue-derived mesenchymal stem cells (ATSCs) have been used as an alternative to bone marrow-derived mesenchymal stem cells (BMSCs) for bone tissue engineering applications. The ability of ATSCs to promote new bone formation remains lower than that of BMSCs. This study aimed to investigate the mechanisms underlying osteogenicity differences between human ATSCs and BMSCs in ceramic constructs, focusing on the effects of inflammation on this process. In contrast to ATSC-containing constructs, which did not induce bone formation in an ectopic mouse model, BMSC constructs consistently did so. Gene expression analysis revealed that human BMSCs, concomitantly with host murine progenitors, differentiated into the osteogenic lineage early post-implantation. In contrast, ATSCs differentiated later, when few implanted viable cells remained post-implantation, while the host murine cells did not differentiate. Comparison of the inflammatory profile in the cell constructs indicated concomitant upregulation of some human and murine inflammatory genes in the ATSC-constructs compared to the BMSC-constructs during the first-week post-implantation. The high level of chemokine production by the ATSCs was confirmed at the gene and protein levels before implantation. The immune cell recruitment within the constructs was then explored post-implantation. Higher numbers of TRAP-/ MRC1 (CD206)+ multinucleated giant cells, NOS2+ M1, and ARG1+ M2 macrophages were present in the ATSC constructs than in the BMSC constructs. These results proved that ATSCs are a transient source of inflammatory cytokines promoting a transient immune response post-implantation; this milieu correlates with impaired osteogenic differentiation of both the implanted ATSCs and the host osteoprogenitor cells.

Introduction:

Bone tissue engineering aims at inducing the regeneration of functional bone tissue using scaffolds (including allo/xenogenic bone tissue, natural or synthetic materials [1]) combined with bioactive factors and/or stem cells as an alternative to bone grafting. Mesenchymal stem cells (also known as "multipotent stromal cells" or MSCs) are the most appealing cell source in tissue engineering therapeutic approaches because of their fundamental role in tissue homeostasis and injury repair [2]. Inherent advantages of MSCs for tissue engineering applications are the possibility of harvesting from various body organs and tissues, including bone marrow, adipose tissue, synovium, dental pulp, cord blood, umbilical cord, etc. [3–5]. Moreover, MSCs have a robust clonal self-renewal and multilineage differentiation potential, including the osteogenic lineage [3, 6, 7]. Although bone marrow (a natural reservoir of bone cell progenitors) has been the

main source of MSCs for bone tissue engineering applications [8], other sources have been investigated because the number of MSCs in the bone marrow is low (0.001%–0.01% of the total mononuclear cell fraction [3]) and because bone marrow collection from the iliac crest is an invasive procedure. Adipose tissue is an interesting alternative to bone marrow since it contains approximately 500-fold more MSCs [9], and tissue pertinent collection from several anatomical sites is possible with minimum patient discomfort.

Adipose tissue-derived MSCs (ATSCs) and bone marrow-derived MSCs (BMSCs) share several features, such as the expression of specific surface markers, which are characteristic of the MSCs, and capability for multilineage differentiation, including the adipogenic, chondrogenic, myogenic, and osteogenic lineages [10]. Like BMSCs, ATSCs also exhibit high paracrine activity through the secretion of several bioactive molecules (such

as growth factors and miRNAs), which can exert angiogenic and homing activity toward endogenous progenitor cells in vivo [11, 12]. For all the aforementioned reasons, the efficacy of ATSCs from various species for regenerating bone has been investigated in in vivo studies (see Storti, et al., for review [13]). In comparison with the BMSCs, however, the osteogenicity of the ATSCs remains debatable since inconsistent results have been reported using in vivo bone defect models. While some studies reported similar regenerative capabilities for ATSCs and BMSCs [14–17], others reported greater regenerative capacity for the BMSCs [18–21]. Moreover, most studies assessing the intrinsic in vivo osteogenic capability of ATSCs using ectopic models, in which resident differentiated osteogenic cells cannot contribute to bone formation, provided evidence of either lack or minimal bone formation [22], unless the ATSCs were previously primed using either biomolecules (such as steroid hormones and bone morphogenetic proteins) or genetic manipulation promoting the osteogenic differentiation [23–25]. In contrast, un-primed BMSC routinely form ectopic bone [22, 26–28]. So far, the underlying mechanisms of the attenuated osteogenicity of ATSCs have been poorly investigated.

It is acknowledged that MSC-related clinical efficacy relies not only on their direct role on new tissue formation (because of their capability to differentiate into functional tissue cells), but also their indirect role in stimulating resident progenitor cells via a trophic activity [29]. In fact, the MSC capability to release numerous immunomodulatory, angiogenic, chemotactic, and differentiating factors is considered more important for tissue repair than MSC engraftment and differentiation at the site of lesions. Among their paracrine properties, the MSC capability to dampen innate and adaptive immune responses is critical for facilitating their regenerative potential [30–32]. Among their various immunomodulatory effects, MSCs promote switching from the proinflammatory (M1) to the anti-inflammatory (M2) macrophage phenotype, enhance neutrophil survival, favor the generation of regulatory dendritic cells, and inhibit NK cell-mediated cytotoxicity [12, 33, 34]. MSCs are combined with synthetic material scaffolds in bone regeneration applications, usually bioceramic. The implanted materials promote responses from various innate immune cells (including mast cells, neutrophils, monocytes, macrophages, and multinucleated giant cells (MNGCs)), which regulate inflammation and contribute to the cascade of bone-healing processes [35, 36]. Despite the MSC immunomodulatory properties [37–39], their exact role in the innate immune response during bone formation mediated by the MSCs contained in material constructs remains undetermined.

For the aforementioned reasons, the present study investigated aspects of the underlying mechanism differences in ATSC and BMSC osteogenicity in tissue-engineered constructs by exploring the effects of the innate immune response. While other studies assessed the immunomodulatory effect of ATSCs, to the best of our knowledge, no other study to date has investigated the inflammatory milieu of ATSC-containing constructs in vivo.

Materials and Methods:

Mesenchymal stem cell cultures

Human bone marrow-derived MSCs (BMSCs) were harvested from bone marrow from 3 donors (1 woman and 2 men; 15, 22 and 31 years-old, respectively) at the Lariboisiere Hospital, Paris, France. BMSCs were isolated from each donor's bone

marrow using a procedure adapted from literature reports [40]. Adipose tissue-derived MSCs (ATSCs) from 3 donors (of unknown gender and age) were purchased from Poietics™ (Lonza). Both BMSCs and ATSCs were cultured in α -Minimum Essential Medium (α -MEM, Sigma) containing 10% fetal bovine serum (FBS; PAA Laboratories) and 1% antibiotics (PAA Laboratories) (standard culture medium). The BMSCs and ATSCs from each donor were cultured separately (up to passage 6), tested for mycoplasma contamination, and characterized for their proliferative doubling time (6.4 ± 1.6 days and 2.0 ± 0.8 days for the BMSCs and ATSCs, respectively) and their expression of select CD markers (specifically, positive for CD90, CD73, CD105, and negative for CD14, CD45, CD31, and CD146). The respective potentials for differentiation into osteogenic and adipogenic lineages were also determined in vitro for the BMSCs and ATSCs from each donor, as previously described [27]. BMSCs and ATSCs from their respective three donors were separately expanded and pooled at an equal ratio just before use in the experiments described in this manuscript.

Animals

Twenty four 8-week-old female Rj;NMRI-Foxn1nu/Foxn1nu nude mice obtained from JanvierLabs were used for all animal experiments conducted in the present study. The animals were handled following the European Directive 2010/63/EU regarding the protection of animals used for scientific purposes. After intake in our laboratory, mice were housed (3 mice per cage enriched with a nest igloo and wooden chew bars) at a constant room temperature of 22°C and had water and food ad libitum. The protocols of in vivo experiments were approved by the local Ethics Committee (N°9 Villemin) on Animal Research and then authorized by the French Ministry of Agriculture (agreement number APAFIS#16561-2018071215383152).

In vivo determination of the osteogenic potential of BMSCs and ATSCs

Preparation of cell-containing constructs: Coral granules (200–400 μ m diameter; Porites species; Biocoral®, Inotek, Inc) were used as scaffolds. This biomaterial was chosen because it has previously been employed successfully in preclinical studies assessing MSC-containing constructs in treating bone defects [41–43]. Granule aliquots (each 40 mg) were sterilized at 150°C for 2 hours, and washed using standard culture medium at 37°C for 1 hour. Either pooled BMSCs or pooled ATSCs (106 cells suspended in culture medium) were then seeded onto the coral granules and allowed to adhere at 37°C overnight. Before implantation, the cell-seeded granules were embedded in a fibrin gel prepared by mixing fibrinogen (18 mg/mL) with thrombin (5 U/mL). These cell-containing constructs were maintained in 2 mL of standard cell culture medium at 37°C until implantation.

In vivo implantation: In a first set of experiments, the in vivo osteogenic potential of BMSC- or ADSC-containing constructs (n=8 for each cell type) were compared. The constructs were subcutaneously implanted in mice, as previously described [44]. Briefly, each mouse was preoperatively given analgesics (0.4 mg of buprenorphine per kg animal weight; Axience), anesthetized by intraperitoneal injection of 100 mg.kg⁻¹ ketamine (Ketalar; Virbach) and 10 mg.kg⁻¹ xylazine (Rompun 2%; Bayer). After

disinfection of the animal skin, symmetrical incisions were made on the back of each mouse on both sides of the spine, subcutaneous pouches were formed, and one cell-containing construct was randomly inserted per pouch (four constructs per mouse). The skin at the incision sites was closed using interrupted non-resorbable sutures. All animals were monitored until complete recovery. Thereafter, the animals were monitored twice a day for 3 days, then once a day for 3 days, and finally twice a week until the end of the experiment. The humane endpoints were weight loss (20%), altered general behavior, and infected implantation site, but none were reached.

Micro-computerized tomographic analysis, histology, histomorphometry, immunohistochemistry

At eight weeks post-implantation, the mice were sacrificed using an overdose of barbiturate (Dolethal®; Vetoquinol), and the retrieved TE-constructs were immediately fixed using 10 % neutral buffered formaldehyde solution for 24 hours. The fixed specimens were then imaged using a high-resolution micro-computerized tomography (μ -CT) machine (Skyscan 1172; Bruker) at the following settings: pixel size = 6 μ m; source voltage = 40 kV; source current = 100 μ A; no filter; rotation step = 0.3°; and exposure time = 340 ms. The collected images were reconstructed using NRecon software (Bruker). They were used to determine the volumes of both newly formed bone and remaining (not resorbed) coral using CTan software (Bruker) with binarization thresholds for bone and coral determined by Otsu's method. Each excised construct was then processed for undecalcified histology and tissue sections were stained with Picrofuchsin and Stevenel's blue. The bone surface area (stained in red) was measured in each specimen section and expressed in mm² according to established methods [45].

Another set of BMSC- and ATSC-containing constructs and cell-free constructs (coral group) were implanted (n=4 per group) as previously described to examine the explants at earlier post-implantation time points. After 14- and 28-days post-implantation, the constructs were explanted, fixed in 4% paraformaldehyde (pH 7.4) for 24 hours, decalcified using ethylenediaminetetraacetic acid (14.5% w/v) at 4°C for 1 week, and embedded in paraffin. Sequential 7 μ m sections of each construct were obtained, and were stained with Hemotoxylin Eosin (HE); the surface area and number of vessels as well as the number of multinucleated giant cells present on each section were counted manually using ImageJ. Tartrate-resistant acid phosphatase (TRAP) staining was also performed using a commercial-available staining kit (Acid Phosphatase Leukocyte Staining Kit, Sigma) and following the manufacturer's instructions. Other sequential sections were processed for immunohistological determination of human beta-2-microglobulin (B2M, a membrane protein that enables tracking human cells), murine CD86, murine NOS2 (nitric oxide synthase 2), murine ARG1 (arginase 1) and murine mannose receptor C type 1 (MRC1/CD206) markers. The sections were heated at 95°C with 10 mM citrate buffer, pH 6.0 for 5 min for all immunostainings. For CD68 and ARG1 labeling, after rinsing in tris-buffered saline (TBS), blocking with 5% goat serum, and rinsing again in TBS, tissue sections were incubated with either the monoclonal anti-CD86 antibody conjugated to Alexa® 647 (sc-28347 AF647, Santacruz, 1:100) or the anti-ARG1 antibody conjugated to Alexa® 647 (sc-271430- AF647, Santacruz, 1:50), respectively, at 4°C overnight. After rinsing in PBS, sections were counterstained with 4',6-diamidino-2-phenylindole (DAPI,

1/100,000). Images were captured using a Nikon TE2000 with Aurox clarity laser-free confocal microscope. 'Positive' cells were determined by creating a threshold for fluorescence intensity. For NOS2 and MRC1 labeling, after removing the endogenous peroxidase with 3% H₂O₂, rinsing in tris-buffered saline (TBS), blocking with 10% bovine serum albumin, and rinsing again in TBS, the sections were incubated with either polyclonal rabbit anti-beta-2-microglobulin (1/1000) at room temperature for 1 hour (NCL-B2Mp; Novocastra), polyclonal rabbit anti-NOS2 antibody (1/50) at 4°C, overnight (ab15323; Abcam) or polyclonal rabbit anti-MRC1 antibody (dilution 1/1000, at 4°C, overnight (ab64693; Abcam). Each section was then rinsed in PBS, incubated with the Labelled Polymer-HRP Anti-Rabbit antibody (Envision+ Kit, Dako) for 30 min, and then visualized using the DAB chromogen (Dako) for 5 minutes and counterstained with Harris hematoxylin for 30s.

Gene expression analysis using RT-qPCR of cell contained in constructs

Other specimens of both BMSC- and ADSC-containing constructs (as well as cell-free, coral constructs) were prepared and either non-implanted (day 0) or implanted for 7, 14, and 28 days (n=6 per group), excised, snap-frozen in nitrogen liquid and stored at -80°C. The frozen excised constructs were then finely chopped (using a scalpel blade), and the contained total RNA was extracted by adding 1 mL of Trizol® (Thermoscientific). The RNA concentration and purity were determined using a NanoDrop spectrophotometer (NanoDrop 1000, Labtech). cDNA was obtained after reverse transcription of 3 μ g of purified RNA using the Superscript II enzyme (Invitrogen) and random primers. Quantitative Polymerase Chain Reaction (QPCR) was then performed using 25 ng and 75 ng cDNA (iCycler iQ PCR plates; Biorad) and Taqman gene expression assays (Life Technologies) for mouse genes and human genes, respectively, following the manufacturer's instructions and using the MyiQ™ Real-Time PCR Detection System (Biorad). The results were normalized to those of the respective ACTB and Actb as reference genes. These reference genes were selected following a study comparing the stability of 5 candidate reference genes using the web-based RefFinder tool (<https://blooge.cn/RefFinder/>) that integrates the currently available major computational programs (geNorm, Normfinder, BestKeeper, and the comparative Δ -Ct method) to compare and rank the tested candidate reference genes [46]. The full names of the genes monitored and the assay IDs are given in the Supplementary Table 1, and the MIQE checklist is presented in the Supplementary Table 2.

The gene expression profile of human cytokines and chemokines in non-implanted cell-containing constructs was analyzed using a RT² Profiler PCR array (PAHS-150Z, Qiagen) following the manufacturer's instructions. Briefly, the RNA isolated from cell constructs was further purified using RNeasy Mini Kits (Qiagen), and cDNA was then synthesized from 500 ng RNA. cDNA from each replicate (n = 6 per group) was equally pooled to yield 500 ng total RNA for each cell type and was used to perform the RT-qPCR. Gene expression levels were analyzed and compared between the 2 groups using the web-based software «RT² Profiler PCR Array Data Analysis version 5.1» (Qiagen). Induction \geq 3.0 and \leq -3.0 were defined as cut-off values. Expressions of the highest upregulated and downregulated select genes were further validated on each individual replicate (n=6) for each cell type using Taqman hydrolysis probes.

In vitro inflammatory profile of cell contained in constructs

The hIL6, hIL8, hIL1B, hILA, hILRN, hCSF3, hCCL5, hCXCL5, hCCL20, hCXCL10 chemokines, and cytokines released from ATSC- and BMSC-containing constructs after 48 hours of culture in α -MEM containing 0.5% Bovine serum albumin (conditioned supernatant media named either ATSC-CM or BMSC-CM) were quantified using Luminex technology (R&D Systems).

Real-time migration of macrophage in response to ATSC-CM or BMSC-CM was assessed using an IncuCyte® S3 system (Sartorius). Human peripheral blood mononuclear cells (PBMCs) were isolated from human blood (obtained from the Etablissement Français du Sang) and cultured using a standard culture medium supplemented with 50 ng/ml macrophage colony-stimulating factor 1 (CSF1) for 6 days to generate macrophages. Collected macrophages were plated in α -MEM/0.5% FBS in ClearView chemotaxis 96-well insert plate (2,000 cells/well pre-coated with 50 μ g/ml Matrigel (Corning)). 200 μ l of either ATSC-CM, BMSC-CM, or α -MEM/2% FBS (as control medium) were added to the bottom reservoir. The plate was then incubated into the IncuCyte® S3 instrument at 37 °C. Images of each well's top and bottom sides were captured every hour for 48 hours. The total area occupied by macrophages migrated onto the bottom surface of each well was normalized by the respective area on the top occupied by cells at the beginning of the experiment (t = 0) (n = 4 per condition) using IncuCyte® analysis V2020B software (Sartorius).

Statistical analyses

Statistical analyses were performed using a commercially available software package (GraphPad Prism, version 9.4.0; GraphPad Software, Inc). Quantitative data were expressed as mean \pm Standard error of the mean (SEM). The t-test (for normally distributed variables) or Mann-Whitney test was used to compare the means of two data groups. The one-way analysis of variance (ANOVA) followed by Tukey's post hoc test was used to compare the means of more than two data groups. The quantitative kinetics data were analyzed using two-way ANOVA followed by Tukey's post hoc test. For all analyses, differences at p < 0.05 were considered statistically significant

Results

ATSC and BMSC characterization

The surface phenotype of ATSCs and BMSCs was determined using flow cytometry and characteristic markers of human MSCs. More than 99% of the BMSC and ATSC populations from the respective three donors tested exhibited the CD45-, CD14-, CD31-, CD146-, CD90+, CD73+, and CD105+ markers. The exception was a difference in the expression of CD105+ by one BMSC donor and one ATSCs donor, which was 87 % and 76 %, respectively (Supplementary Figures 1A-B). The BMSCs and ATSCs from all three donors differentiated into the osteogenic and adipogenic lineages, albeit varying degrees for each donor (See Supplementary Figures 2A-B).

In vivo osteogenic potential of the implanted MSCs

While all the BMSC-containing constructs exhibited bone formation, the ATSC-constructs induced no bone tissue formation (Figure 1A). Histomorphometric analyses confirmed the μ -CT quantification results (Figure 1B). In addition, the remaining coral volume in the BMSC-constructs was significantly lower than the one observed in the ATSC-constructs (Figure 1C). The resorption levels were 85% for the BMSCs and 59% for the ATSCs. Representative images of histology sections from each type of construct tested are shown in Figure 1D. Large areas of new bone enclosing bone marrow-like tissue deposited around residual coral granules were observed in the BMSC-containing constructs (Figure 1Di-ii). In contrast, no bone tissue was observed in the ATSC-containing constructs (Figure 1 Diii) and images at higher magnification revealed the presence of numerous multinucleated giant cells (MNGCs) in contact with the coral material (Figure 1 Div).

In vivo engraftment of human MSCs contained in the constructs

To estimate the numbers of the residual human MSCs in the implanted constructs, a kinetic analysis of the expressed human ACTB gene by the implanted MSCs in constructs explanted at 0, 7, 14, and 28 days post-implantation was performed. These results were expressed as the ratio of the level of human ACTB to that of the 18S (expressed by both human and murine cells) (Figure 2A), giving an estimate of the ratio between human and all (human and murine) cells contained within constructs. A fast and significant decrease of the (mRNA) ACTB expression was observed by both cell types tested over time, although to a lesser extent by BMSCs compared to ATSCs; their respective expression levels on day 28 were 14% and 1 % of the expression levels on day 0, but no statistical difference between both groups was observed. Immunostaining of human β 2-microglobulin confirmed the presence of implanted human MSCs remaining in the explanted cell constructs 14- and 28-days post-implantation (Figures 2Ci-iv). Positive cells were present in both types of cell constructs, but in greater numbers in the BMSC- than in the ATSC-containing constructs on day 28 post-implantation (Figures 2Ciii and 2Civ). Quantification of the positive staining indicated a not significant trend towards higher cell engraftment for the BMSC- than for ATSC-containing constructs 28 days post-implantation (Figure 2B). It should be noted that the bone tissue formed within the BMSC-containing constructs was hybrid with the presence of a few human labeled cells (arrows in Figure 2Ciii) and numerous murine unlabeled cells in osteocyte lacunae.

Because the rate of neovascularization within the cell-containing constructs impacts the viability of implanted MSCs, the surface area and number of vessels in each section were quantified (Figure 2D). The results showed that these two quantifications were higher in the ATSC constructs on day 28 than in the other constructs, indicating greater vascularization in the ATSC constructs.

In vivo osteogenic differentiation of both implanted MSCs and recruited host progenitors in the cell-containing constructs

Kinetic analyses for the expression of human and murine genes were performed using species-specific primers in order to

determine the osteogenic commitment of both the grafted MSCs and the recruited mouse (host) progenitors within the constructs post-implantation. The analysis of the human genes revealed, in comparison to the BMSC group, an upregulation of the early RUNX family transcription factor 2 (RUNX2) in the ATSC group 28 days post-implantation (Figure 3A). In contrast, expression of the SP7 transcription factor (also named Osterix) and of the early osteogenic markers alkaline phosphatase, biomineralization associated (ALPL) and integrin binding sialoprotein (IBSP) highly increased in BMSC-constructs at day 28, but was either absent or weakly expressed in the ATSC-constructs (Figure 3A). Similarly, expression of the murine osteogenesis-related genes (mRNA) Runx2, Sp7, Alpl, and Ibsp increased in the BMSC-constructs on day 28; it should be noted that Runx2 (which is most highly expressed in BMSC constructs at a time when bone tissue with marrow is observed) has also been reported to be expressed in hematopoietic stem cell compartment present in the bone marrow [47]. In contrast, the expression of the aforementioned osteogenic-related genes in the ATSC-constructs remained as low or lower as that observed in the cell-free constructs (Coral group)(Figure 3B). Expression of murine (mRNA) Calcr, the osteoclast-associated calcitonin receptor, was also upregulated in the BMSC-constructs with the duration of implantation. All these data provided evidence that, upon implantation, the BMSCs were committed towards the osteogenic lineage concomitantly with the host murine progenitors; an osteoclastic activity by host murine cells also occurred within the cell constructs, and all these events led to the formation of new bone. In contrast, osteogenic differentiation of the implanted ATSCs started at a later time (specifically, 28 days post-implantation) in the absence of murine host progenitor differentiation and osteoclastic activity.

The in vivo and in vitro inflammatory environment in the MSC-containing constructs

The in vivo inflammatory microenvironment within the ATSC- and BMSC-containing constructs (Figures 4A-4B) was then investigated. Compared with the results obtained from BMSC constructs, expression of the three human proinflammatory cytokines interleukin 1 beta (IL1B), interleukin 6 (IL6), and colony stimulating factor 3 (CSF3) were upregulated in the ATSC constructs before implantation and after 7 days of implantation. After 2 weeks of implantation, though, the gene expressions between the two groups were similar. It should be noted that the proinflammatory tumor necrosis factor alpha (TNF) gene was not detected post-implantation by either type of the MSCs tested (data not shown). In parallel, expression of the murine (mRNA) Il1b and Tnf genes, was also significantly upregulated in the ATSC-constructs compared to BMSC-constructs during the first week of implantation (Figure 4B); expression of the murine (mRNA) Il6 gene was also upregulated during the first week of implantation, but no difference was observed between groups (Figure 4B).

An extensive human cytokine and chemokine PCR analysis comparing the ATSCs and BMSCs contained in constructs at day 0 was performed to determine the inflammatory profile of these cells before implantation. These results revealed up-regulation of 23 out of 84 genes tested in the ATSCs compared to the BMSCs (Figure 5A and Supplementary Table 3). TaqMan-based RT-qPCR confirmed that the highest (> 30-fold) upregulated genes in ATSCs were CSF3, CXCL11, CXCL10, and CXCL5, while the moderately (from 2- to 10-fold) upregulated genes were the IL1b, IL6, CCL5, IL1ra, CXCL8, CCL20, and IL1a genes. It is worth

noting that the CXCL12, TNFSF1 (RANKL), and BMP4 genes were (from 10- to 24-fold) upregulated in BMSCs compared to ATSCs (Figure 5B).

The secretory profile of construct-contained ATSCs was then compared with that of BMSCs by assessing the concentrations of cytokines in the supernatants from 48-hour cultures. Concentrations in ATSC-conditioned media were significantly higher for CSF3 (64 fold), CXCL5 (13 fold), IL1A (5.4 fold), IL1RN (5.4 fold), IL1B (4.0 fold), CCL20 (3.7 fold), CCL5 (2.7 fold), IL6 (2.3 fold), and IL8 (2.3 fold) but not for CXCL10 molecules (Figure 5C). Because the components of the ATSC secretome included numerous chemokines, the macrophage chemotactic potential of these conditioned media was assessed and compared. PBMC-derived macrophages were recruited more efficiently by the conditioned media from ATSCs compared to that from BMSCs (Figure 5D). Altogether, these results provided evidence that the ATSCs are a source of proinflammatory cytokines/chemokines, which affect macrophage functions such as migration.

In vivo immune cell recruitment within cell-containing constructs

The stronger inflammatory environment created by ATSCs in constructs prompted further analysis of the in vivo recruitment of immune cells. The presence of numerous giant cells revealed within the ATSC-containing constructs excised after 8 weeks post-implantation (Figure 1Div) was confirmed in constructs excised after 28 days post-implantation (Figure 6A). In order to resolve whether the observed giant cells were either osteoclasts or foreign body giant cells (i.e., multinucleated giant cells or MNGCs), pertinent tissue sections were stained with TRAP (a marker of osteoclasts) and against the mannose receptor C type 1 (MRC1 or CD206), a MNGC marker [48, 49]). While the giant cells in BMSC-containing constructs were positive to TRAP staining (Figure 6Bi), giant cells in the ATSC-containing constructs were negative to TRAP (Figure 6Bii) and positive to murine MRC1 marker (Figure 6D), indicating the presence of osteoclasts in BMSC-constructs and of MNGCs in ATSC-constructs. It should be noted that TRAP staining in BMSC-constructs was 3.8-fold higher on 14 days than on 28 days post-implantation (Figure 6C).

Recruitment of proinflammatory M1 and pro-regenerative M2 macrophages were also assessed in post-implantation constructs. Expression of the murine Cd68 gene, a pan-macrophage marker, increased with the time of implantation and was found downregulated in ATSC compared to the other groups on day 28 (Figure 7A). Gene expression of the murine Cd86 and nitric oxide synthase 2 (Nos2 also known as iNos) markers and of the murine arginase 1 (Arg1), Il10, and Mrc1 (Cd206) markers were quantified as evidence for the respective presence of M1 and M2 macrophages within the constructs tested (Figure 7A). The expression of murine Cd86 gene remained steady with the time of implantation and was found similar in both cell constructs (and lower than in coral group on day 7) ; in contrast, expression of the murine Nos2 gene decreased in all groups tested with the time of implantation, and it was significantly higher in ATSC-containing constructs compared to BMSC group 7-days post-implantation. Interestingly, expression of the M2-associated murine Arg1 gene also decreased in all groups tested with the time of implantation, and was also upregulated in the ATSC- containing constructs compared to the BMSC-containing and to the cell-free constructs

on day 7 post-implantation (Figure 7A). Expression of both the murine *Il10* and *Mrc1* (*Cd206*) genes was similar in both the cell-containing constructs at all post-implantation times (Figure 7A).

The presence of M1 and M2 macrophage markers was confirmed by immunohistologic analysis of the implanted constructs (Figures 7B-F), with results comparatively consistent with those obtained from gene expression analysis. For the M1 markers, immunostaining for murine CD86 (Figures 7B) and its quantification (Figures 7F) revealed similar numbers of CD86-positive cells in both cell-containing constructs, with higher overall labeling than in cell-free constructs; the labeling decreased with the time of implantation. NOS2 immunostaining revealed the presence of a higher number of NOS2-positive cells in the ATSC-constructs compared to BMSC- and cell-free constructs on both post-implantation time points tested (Figures 7C and 7F). For the M2 markers, immunostaining for ARG1 also showed higher labeling in ATSC constructs on day14 post-implantation (Figures 7D and 7F), whereas the MRC1 immunostaining revealed the presence of MRC1-positive (including giant) cells in all construct types tested with a non-significant trend of stronger MRC1 staining in both the ATSC and coral groups compared to BMSC group (Figures 7E and 7F). Overall, these results indicated that, compared to the BMSC-containing constructs, the ATSC-containing constructs were devoid of osteoclasts, but contained more MNGCs. In addition, the pattern of macrophage phenotype differed in the MSC-containing constructs, with higher expression of the functional macrophage markers M1 (NOS2+) and M2 (ARG1+) in the ATSC constructs compared to the BMSC constructs (as the expression of macrophage surface marker did not differ).

Discussion:

Bone tissue engineering has made significant progress over the past few years, but there are still several challenges to be overcome before it can be used on a large scale in clinical practice (see [50–52] for reviews). Among the many challenges that will contribute to advancing cell-based engineered constructs are a deeper understanding of stem cell biology and better identification of the biochemical and biophysical environment in tissue constructs that favors cell viability, differentiation, and osteogenesis. In the present study, we provided evidence that, compared to BMSCs, ATSCs are a source of proinflammatory cytokines and chemokines that transiently promotes an inflammatory environment within the cell-containing constructs; this milieu correlates with impaired osteogenic differentiation of both implanted ATSCs and host osteoprogenitors.

The current standard method for assessing the bone-forming potential of a cell population *in vivo* is the ectopic bone formation assay since, in such an environment, no resident osteogenic cells are present and, therefore, the true potential of the implanted cells can be rigorously assessed [53]. Using this ectopic model, we observed, as other previous studies had reported [22–24], the absence of *in vivo* osteogenicity of the ATSCs. In contrast, BMSCs promoted consistent bone tissue formation containing bone marrow territories and numerous osteoclasts. The ATSCs and BMSCs from the 3 donors tested exhibited similar (but at different extends) immunophenotype and capability for *in vitro* osteogenic and adipogenic differentiation confirming the literature report that the *in vitro* osteogenic differentiation does not correlate with the *in vivo* osteogenic potential of these cells [54].

In order to determine the origin of this difference in osteogenicity, the portion of residual human MSCs after implantation was determined. Results indicated a gradual decline of both BMSC and ATSC numbers for the duration of implantation, in agreement with the numerous previous published reports of major loss of MSCs post-implantation [55, 56]. Our data also showed that a small proportion of transplanted human MSCs survived 8 weeks post-implantation with a non-significant trend towards greater post-implantation viability of BMSCs compared to ATSCs. The level of neovascularization within the implants was also assessed by vessel quantification, which was higher for ATSC-containing constructs at day 28 compared to other constructs. This result is consistent with the literature showing that ATSCs enhanced neovascularization compared to BMSCs [22].

We further assessed the osteogenic commitment of both implanted MSCs and recruited host osteoprogenitors within the constructs post-implantation. Our data showed an *in-situ* differentiation of surviving implanted BMSCs into osteoblasts and their direct participation in the new bone formation, as confirmed by the presence of some osteocytes of human origin in the bone tissue mediated by the BMSCs. In addition to their direct contribution, it is well established that, through the release of several chemical compounds with various (including osteogenic) bioactivities, MSCs stimulate endogenous healing by their paracrine activity [24, 57, 58]. Our observations confirmed that implanted BMSCs induced (most likely through their paracrine effects) recruitment and differentiation of host osteoprogenitor cells. In contrast, implanted ATSCs differentiation (evidenced by upregulation of early osteogenic transcription factors) was induced at a later time point (i.e., 28 days post-implantation) than that observed for the BMSCs; at that time point, very few viable ATSCs remained. In addition, no osteogenic commitment of the host progenitor cells occurred in these ATSC-constructs. Altogether, our data provided evidence that ATSCs, which can differentiate into the osteogenic lineage *in vitro*, are transiently prevented from differentiating and recruiting host osteoprogenitors post-implantation. Brennan et al. previously reported the respective occurrence and absence of bone formation after ectopic implantation of either BMSCs or ATSCs; more interestingly, mixing ATSCs with BMSCs decreased the resulting rate of bone formation [22]. These observations suggest the occurrence of a milieu in ATSC-containing constructs that transiently inhibits *in-situ* osteogenic differentiation and/or the release of paracrine signals needed for bone formation.

Because the immune system and bone formation are inherently linked [59, 60], and bioactive factors released by MSCs affect the local immune system [33], this study investigated the role of inflammation on the weaker *in vivo* osteogenicity of the ATSCs compared to that of BMSCs. Since innate immune responses initiate bone regeneration in the early stage of bone fracture repair, the present study focused on this specific immune response. It should be noted that the immunocompromised Nude mice (in which the cell-containing constructs were implanted), are athymic and, thus, have fewer T cells but intact innate immunity [61]. Our results provided evidence for the upregulation of proinflammatory human cytokines (such as IL1B, IL6, and CSF3) in ATSC- compared to BMSC-containing constructs during the first week of implantation. The stronger inflammatory profile of ATSCs contained in the constructs was also confirmed before implantation using an extensive PCR array. Such cytokine upregulation was confirmed by the protein levels in the supernatants of ATSC-containing constructs *in vitro*. Several

studies from the literature have reported that, like other MSCs, ATSCs exhibit a potent paracrine function, even stronger than the one exhibited by the BMSCs [12, 62]. ATSCs and BMSCs affect both the innate and adaptive immune system by suppressing the local immune system, modulating T and B cells, and inducing expression of anti-inflammatory chemical compounds, such as IL10, IL1RN, prostaglandin E2, or indoleamine-pyrrole 2,3-dioxygenase (IDO) [12]. In this study, compared to values obtained with BMSCs, IL1RN was indeed overexpressed in ATSCs; (mRNA) IL10, however, was not expressed by any type of the MSCs tested (data not shown). It should be noted that the transcriptomic and secretomic MSC analyses were performed on cells loaded with coral granules taking into consideration the impact of the material on the cellular response; on the contrary, most of the analyses reported in the literature were obtained from MSCs cultured in 2D on tissue culture plastic; these different methodologies may lead to variations in the profiles of both ATSCs and BMSCs.

An important observation of the present study is that the inflammatory cytokines and chemokines secreted by implanted ATSCs promoted a transient inflammatory environment within the constructs during the first-week post-implantation. Such a milieu induced the in-situ recruitment of immune cells, as confirmed in vitro and in vivo. Specifically, the ATSC (rather than the BMSC) secretome recruited more efficiently PBMC-derived macrophages in vitro. In vivo, ATSC-containing constructs exhibited significantly increased recruitment of MNGCs; they also promoted the polarization of M0 macrophages towards proinflammatory M1 macrophages and, more surprisingly, pro-regenerative M2 macrophages and/or their recruitment. Growing evidence from the literature suggests that macrophages significantly impact osteogenesis during bone regeneration, though the underlying mechanisms have not yet been fully elucidated. The current understanding is that M1 macrophages are necessary for initiating the proinflammatory phase during bone repair [63] and during the process of MSC-based osteoinduction [37, 38]. Through their immunomodulatory effects on macrophages, transplanted MSCs mitigate chronic inflammation by switching from the M1 to the M2 phenotype. The M1/M2 macrophage phenotype balance and, therefore, the precise timing of the M1-to-M2 transition, are critical for the resolution of inflammation towards appropriate MSC-induced osteogenesis (see [64, 65] for reviews).

Osteoclasts also play a central role in osteogenesis since their depletion impeded bone formation in a similar tissue engineering ectopic model [38]. In the present study, osteoclasts were observed in large numbers in the BMSC-containing constructs at 14 days post-implantation, prior to the appearance of new bone, but they were completely absent in the ATSC-containing constructs; these results confirmed the close relationship between osteoclasts and BMSC-mediated bone formation. In contrast, numerous multinuclear giant cells (MNGCs) were observed in the ATSC-containing constructs. MNGCs and osteoclasts have a common origin and similar morphology but distinct marker patterns [48]. The fusion of macrophages and commitment into either osteoclasts or MNGCs in the presence of synthetic biomaterials and, in response to stem cell-containing constructs, remains poorly understood [49]. In a recent review, Humbert et al. proposed that, through their immunomodulatory properties, MSCs favor osteoclastogenesis instead of MNGC formation, thus promoting new bone formation via recruitment and differentiation of osteoprogenitors [39].

While the relationship between the immune system and bone repair is becoming better described, the mechanisms underlying the role of immune cells in MSC-mediated osteogenesis are still poorly understood. Although this study does not elucidate the exact underlying mechanism behind the difference in osteogenic potential between BMSCs and ATSCs, it has provided evidence that ATSCs are a transient source of inflammatory cytokines that promote a transient immune response after implantation, an event that correlates with impaired osteogenic differentiation. Other factors may also contribute to the greater osteogenic potential of BMSCs compared to ATSCs; in particular, slightly better survival of implanted BMSCs and/or a BMSC secretome more favorable for promoting osteogenesis; in particular, we observed overexpression of CXCL12 (known to be involved in MSC recruitment) and BMP4 (which is an osteoinductive factor).

Conclusion

The present study provided novel evidence that, compared to BMSCs, ATSCs secreted more cytokines and chemokines, which transiently induced an acute inflammatory microenvironment within constructs post-implantation; the result is a milieu characterized by the recruitment of more M1 and M2 macrophages and the commitment of fused macrophages into MNGCs rather than into osteoclasts. These local immune responses temporarily inhibited the osteogenic differentiation of both the implanted ATSCs and the host osteoprogenitors. When this immune response was attenuated, the ATSCs began their osteogenic differentiation, but at a post-implantation time point when their numbers were insufficient to induce either bone formation or differentiation of host osteoprogenitors. These data provide new insight regarding use of ATSCs for bone regeneration applications, while acknowledging the substantial potential of BMSCs for bone repair.

Acknowledgments

The authors thank Prof. Rena Bizios for reviewing the manuscript; the Technology Platform at Institut de Recherche Saint-Louis (IRSL) (Paris) for access to the Incucyte device; Vincent Contremoulins, Emeline Rascussery and Sacha Kuzniak for their technical help in histology analysis. This study was supported by the Fondation de l'Avenir, France (Grant 2017-AP-RM-17-003).

Disclosure Statement

The authors declare no competing financial interests.

Ethics Approval and Consent to Participate: All animal studies were conducted in accordance with the European Directive 2010/63/EU regarding the protection of animals used for scientific purposes. The protocols of in vivo experiments were approved by the local Ethics Committee (N°9 Villemin) on Animal Research and then authorized by the French Ministry of Agriculture (agreement number APAFIS#16561-2018071215383152). Human bone marrow-derived MSCs were harvested from bone marrow obtained as discarded tissue during routine bone surgery at the Lariboisiere Hospital, Paris, France. The tissues were collected with the respective donor's consent in agreement with Lariboisiere Hospital regulations. Adipose tissue-derived MSCs were purchased from Poietics™ (Lonza).

Consent for Publication: Not applicable.

References

- Govoni, M., Vivarelli, L., Mazzotta, A., Stagni, C., Maso, A., & Dallari, D. (2021). Commercial Bone Grafts Claimed as an Alternative to Autografts: Current Trends for Clinical Applications in Orthopaedics. *Materials*, 14(12), 3290. <https://doi.org/10.3390/ma14123290>
- Verfaillie, C. (2002). Adult stem cells: assessing the case for pluripotency. *Trends in cell biology*, 502–8.
- Pittenger, M. F., Mackay, A. M., Beck, S. C., Jaiswal, R. K., Douglas, R., Mosca, J. D., ... Marshak, D. R. (1999). Multilineage Potential of Adult Human Mesenchymal Stem Cells. *Science*, 284(5411), 143–147. <https://doi.org/10.1126/science.284.5411.143>
- Zuk, P. A., Zhu, M., Mizuno, H., Huang, J., Futrell, J. W., Katz, A. J., ... Hedrick, M. H. (2001). Multilineage Cells from Human Adipose Tissue: Implications for Cell-Based Therapies. *Tissue Engineering*, 7(2), 211–228. <https://doi.org/10.1089/107632701300062859>
- Sudo, K., Kanno, M., Miharada, K., Ogawa, S., Hiroshima, T., Saijo, K., & Nakamura, Y. (2007). Mesenchymal Progenitors Able to Differentiate into Osteogenic, Chondrogenic, and/or Adipogenic Cells In Vitro Are Present in Most Primary Fibroblast-Like Cell Populations. *STEM CELLS*, 25(7), 1610–1617. <https://doi.org/10.1634/stemcells.2006-0504>
- Dennis, J. E., Merriam, A., Awadallah, A., Yoo, J. U., Johnstone, B., & Caplan, A. I. (1999). A quadripotential mesenchymal progenitor cell isolated from the marrow of an adult mouse. *Journal of Bone and Mineral Research*, 14(5), 700–709.
- Sacchetti, B., Funari, A., Michienzi, S., Di Cesare, S., Piersanti, S., Saggio, I., ... Bianco, P. (2007). Self-Renewing Osteoprogenitors in Bone Marrow Sinusoids Can Organize a Hematopoietic Microenvironment. *Cell*, 131(2), 324–336. <https://doi.org/10.1016/j.cell.2007.08.025>
- Marolt, D., Knezevic, M., & Vunjak-Novakovic, G. (2010). Bone tissue engineering with human stem cells. *Stem Cell Research & Therapy*, 1(2), 10. <https://doi.org/10.1186/srct10>
- Raposo, E., Bonomini, S., & Calderazzi, F. (2016). Isolation of autologous adipose tissue-derived mesenchymal stem cells for bone repair. *Orthopaedics & Traumatology: Surgery & Research*, 102(7), 909–912. <https://doi.org/10.1016/j.otsr.2016.07.006>
- Zuk, P. A., Zhu, M., Ashjian, P., De Ugarte, D. A., Huang, J. I., Mizuno, H., ... Hedrick, M. H. (2002). Human adipose tissue is a source of multipotent stem cells. *Molecular Biology of the Cell*, 13(12), 4279–4295. <https://doi.org/10.1091/mbc.e02-02-0105>
- Hsiao, S. T.-F., Asgari, A., Lokmic, Z., Sinclair, R., Disting, G. J., Lim, S. Y., & Dilley, R. J. (2012). Comparative Analysis of Paracrine Factor Expression in Human Adult Mesenchymal Stem Cells Derived from Bone Marrow, Adipose, and Dermal Tissue. *Stem Cells and Development*, 21(12), 2189–2203. <https://doi.org/10.1089/scd.2011.0674>
- Kocan, B., Maziarz, A., Tabarkiewicz, J., Ochiya, T., & Banaś-Ząbczyk, A. (2017). Trophic Activity and Phenotype of Adipose Tissue-Derived Mesenchymal Stem Cells as a Background of Their Regenerative Potential. *Stem Cells International*, 2017, 1–13. <https://doi.org/10.1155/2017/1653254>
- Storti, G., Scioli, M. G., Kim, B.-S., Orlandi, A., & Cervelli, V. (2019). Adipose-Derived Stem Cells in Bone Tissue Engineering: Useful Tools with New Applications. *Stem Cells International*, 2019, 1–18. <https://doi.org/10.1155/2019/3673857>
- Stockmann, P., Park, J., von Wilmowsky, C., Nkenke, E., Felszeghy, E., Dehner, J.-F., ... Schlegel, K. A. (2012). Guided bone regeneration in pig calvarial bone defects using autologous mesenchymal stem/progenitor cells – A comparison of different tissue sources. *Journal of Cranio-Maxillofacial Surgery*, 40(4), 310–320. <https://doi.org/10.1016/j.jcms.2011.05.004>
- Jo, C. H., Yoon, P. W., Kim, H., Kang, K. S., & Yoon, K. S. (2013). Comparative evaluation of in vivo osteogenic differentiation of fetal and adult mesenchymal stem cell in rat critical-sized femoral defect model. *Cell and Tissue Research*, 353(1), 41–52. <https://doi.org/10.1007/s00441-013-1610-1>
- Kim, K.-I., Park, S., & Im, G.-I. (2014). Osteogenic differentiation and angiogenesis with cocultured adipose-derived stromal cells and bone marrow stromal cells. *Biomaterials*, 35(17), 4792–4804. <https://doi.org/10.1016/j.biomaterials.2014.02.048>
- Freitas, G. P., Lopes, H. B., Souza, A. T. P., Oliveira, P. G. F. P., Almeida, A. L. G., Souza, L. E. B., ... Rosa, A. L. (2019). Cell Therapy: Effect of Locally Injected Mesenchymal Stromal Cells Derived from Bone Marrow or Adipose Tissue on Bone Regeneration of Rat Calvarial Defects. *Scientific Reports*, 9(1), 13476. <https://doi.org/10.1038/s41598-019-50067-6>
- Mohamed-Ahmed, S., Fristad, I., Lie, S. A., Suliman, S., Mustafa, K., Vindenes, H., & Idris, S. B. (2018). Adipose-derived and bone marrow mesenchymal stem cells: a donor-matched comparison. *Stem Cell Research & Therapy*, 9(1), 168. <https://doi.org/10.1186/s13287-018-0914-1>
- Bothe, F., Lotz, B., Seebach, E., Fischer, J., Hesse, E., Diederichs, S., & Richter, W. (2018). Stimulation of calvarial bone healing with human bone marrow stromal cells versus inhibition with adipose-tissue stromal cells on nanostructured β -TCP-collagen. *Acta Biomaterialia*, 76, 135–145. <https://doi.org/10.1016/j.actbio.2018.06.026>
- Kargozar, S., Mozafari, M., Hashemian, S. J., Brouki Milan, P., Hamzehlou, S., Soleimani, M., ... Seifalian, A. M. (2018). Osteogenic potential of stem cells-seeded bioactive nanocomposite scaffolds: A comparative study between human mesenchymal stem cells derived from bone, umbilical cord Wharton's jelly, and adipose tissue: OSTEOGENIC POTENTIAL OF MSCS/SCAFFOLDS. *Journal of Biomedical Materials Research Part B: Applied Biomaterials*, 106(1), 61–72. <https://doi.org/10.1002/jbm.b.33814>
- Xu, L., Liu, Y., Sun, Y., Wang, B., Xiong, Y., Lin, W. Li, G. (2017). Tissue source determines the differentiation potentials of mesenchymal stem cells: a comparative study of human mesenchymal stem cells from bone marrow and adipose tissue. *Stem Cell Research & Therapy*, 8(1), 275. <https://doi.org/10.1186/s13287-017-0716-x>
- Brennan, M. A., Renaud, A., Guilloton, F., Mebarki, M., Trichet, V., Sensebé, L., ... Layrolle, P. (2017). Inferior In Vivo Osteogenesis and Superior Angiogenesis of Human Adipose Tissue: A Comparison with Bone Marrow-Derived Stromal Stem Cells Cultured in Xeno-Free Conditions. *Stem Cells Translational Medicine*, 6(12), 2160–2172. <https://doi.org/10.1002/sctm.17-0133>
- Scherberich, A., Müller, A. M., Schäfer, D. J., Banfi, A., & Martin, I. (2010). Adipose tissue-derived progenitors for engineering osteogenic and vasculogenic grafts. *Journal of Cellular Physiology*, 225(2), 348–353. <https://doi.org/10.1002/jcp.22313>
- Ruetze, M., & Richter, W. (2014). Adipose-derived stromal cells for osteoarticular repair: trophic function versus stem cell activity. *Expert Reviews in Molecular Medicine*, 16, e9. <https://doi.org/10.1017/erm.2014.9>
- Kuterbekov, M., Jonas, A. M., Glinel, K., & Picart, C. (2020). Osteogenic Differentiation of Adipose-Derived Stromal Cells: From Bench to Clinics. *Tissue Engineering Part B: Reviews*, 26(5), 461–474. <https://doi.org/10.1089/ten.teb.2019.0225>
- Krebsbach, P. H., Kuznetsov, S. A., Satomura, K., Emmons, R. V., Rowe, D. W., & Robey, P. G. (1997). Bone

- formation in vivo: comparison of osteogenesis by transplanted mouse and human marrow stromal fibroblasts. *Transplantation*, 63(8), 1059–1069.
27. Moya, A., Larochette, N., Bourguignon, M., El-Hafci, H., Potier, E., Petite, H., & Logeart-Avrarmoglou, D. (2018). Osteogenic potential of adipogenic predifferentiated human bone marrow-derived multipotent stromal cells for bone tissue-engineering. *Journal of Tissue Engineering and Regenerative Medicine*, 12(3), e1511–e1524. <https://doi.org/10.1002/term.2571>
 28. Bodhak, S., de Castro, L. F., Kuznetsov, S. A., Azusa, M., Bonfim, D., Robey, P. G., & Simon, C. G. (2018). Combinatorial cassettes to systematically evaluate tissue-engineered constructs in recipient mice. *Biomaterials*, 186, 31–43. <https://doi.org/10.1016/j.biomaterials.2018.09.035>
 29. Baraniak, P. R., & McDevitt, T. C. (2010). Stem cell paracrine actions and tissue regeneration. *Regenerative Medicine*, 5(1), 121–143. <https://doi.org/10.2217/rme.09.74>
 30. Gao, F., Chiu, S. M., Motan, D. a. L., Zhang, Z., Chen, L., Ji, H.-L., ... Lian, Q. (2016). Mesenchymal stem cells and immunomodulation: current status and future prospects. *Cell Death & Disease*, 7, e2062. <https://doi.org/10.1038/cddis.2015.327>
 31. Fan, X.-L., Zhang, Y., Li, X., & Fu, Q.-L. (2020). Mechanisms underlying the protective effects of mesenchymal stem cell-based therapy. *Cellular and Molecular Life Sciences*, 77(14), 2771–2794. <https://doi.org/10.1007/s00018-020-03454-6>
 32. Babu, G. S., Badrishi, Y., Oswal, V. M., Jeyaraman, N., Prajwal, G. S., Jeyaraman, M., ... Khanna, M. (2021). Immunomodulatory Actions of Mesenchymal Stromal Cells (MSCs) in Osteoarthritis of the Knee. *Osteology*, 1(4), 209–224. <https://doi.org/10.3390/osteology1040020>
 33. Mattar, P., & Bieback, K. (2015). Comparing the Immunomodulatory Properties of Bone Marrow, Adipose Tissue, and Birth-Associated Tissue Mesenchymal Stromal Cells. *Frontiers in Immunology*, 6. <https://doi.org/10.3389/fimmu.2015.00560>
 34. Rana, N., Suliman, S., Mohamed-Ahmed, S., Gavasso, S., Gjertsen, B. T., & Mustafa, K. (2022). Systemic and local innate immune responses to surgical co-transplantation of mesenchymal stromal cells and biphasic calcium phosphate for bone regeneration. *Acta Biomaterialia*, 141, 440–453. <https://doi.org/10.1016/j.actbio.2021.12.027>
 35. Anderson, J. M., Rodriguez, A., & Chang, D. T. (2008). Foreign body reaction to biomaterials. *Seminars in Immunology*, 20(2), 86–100. <https://doi.org/10.1016/j.smim.2007.11.004>
 36. Sadowska, J. M., & Ginebra, M.-P. (2020). Inflammation and biomaterials: role of the immune response in bone regeneration by inorganic scaffolds. *Journal of Materials Chemistry B*, 10.1039/D0TB01379J. <https://doi.org/10.1039/D0TB01379J>
 37. Tour, G., Wendel, M., & Tcacencu, I. (2014). Bone marrow stromal cells enhance the osteogenic properties of hydroxyapatite scaffolds by modulating the foreign body reaction: BMSCs modulate foreign body reaction. *Journal of Tissue Engineering and Regenerative Medicine*, 8(11), 841–849. <https://doi.org/10.1002/term.1574>
 38. Gambelin, A.-L., Brennan, M. A., Renaud, A., Yagita, H., Lézet, F., Heymann, D., ... Layrolle, P. (2014). Bone tissue formation with human mesenchymal stem cells and biphasic calcium phosphate ceramics: the local implication of osteoclasts and macrophages. *Biomaterials*, 35(36), 9660–7. <https://doi.org/10.1016/j.biomaterials.2014.08.018>
 39. Humbert, P., Brennan, M. A., Davison, N., Rosset, P., Trichet, V., Blanchard, F., & Layrolle, P. (2019). Immune Modulation by Transplanted Calcium Phosphate Biomaterials and Human Mesenchymal Stromal Cells in Bone Regeneration. *Frontiers in Immunology*, 10, 663. <https://doi.org/10.3389/fimmu.2019.00663>
 40. Friedenstein, A. J., Piatetzky-Shapiro, I. I., & Petrakova, K. V. (1966). Osteogenesis in transplants of bone marrow cells. *Development*, 16(3), 381–390.
 41. Petite, H., Viateau, V., Bensaïd, W., Meunier, A., de Pollak, C., Bourguignon, M., ... Guillemain, G. (2000). Tissue-engineered bone regeneration. *Nature Biotechnology*, 18(9), 959–963. <https://doi.org/10.1038/79449>
 42. Manassero, M., Viateau, V., Deschepper, M., Oudina, K., Logeart-Avrarmoglou, D., Petite, H., & Bendsidhoum, M. (2013). Bone Regeneration in Sheep Using Acropora Coral, a Natural Resorbable Scaffold, and Autologous Mesenchymal Stem Cells. *Tissue Engineering Part A*, 19(13–14), 1554–1563. <https://doi.org/10.1089/ten.tea.2012.0008>
 43. Decambon, A., Manassero, M., Bendsidhoum, M., Lecuelle, B., Logeart-Avrarmoglou, D., Petite, H., & Viateau, V. (2017). A comparative study of tissue-engineered constructs from Acropora and Porites coral in a large animal bone defect model. *Bone and Joint Research*, 6(4), 208–215. <https://doi.org/10.1302/2046-3758.64.BJR-2016-0236.R1>
 44. Becquart, P., Cambon-Binder, A., Monfoulet, L.-E., Bourguignon, M., Vandamme, K., Bendsidhoum, M., ... Logeart-Avrarmoglou, D. (2012). Ischemia Is the Prime but Not the Only Cause of Human Multipotent Stromal Cell Death in Tissue-Engineered Constructs In Vivo. *Tissue Engineering Part A*, 18(19–20), 2084–2094. <https://doi.org/10.1089/ten.tea.2011.0690>
 45. Monfoulet, L.-E., Becquart, P., Marchat, D., Vandamme, K., Bourguignon, M., Pacard, E., ... Logeart-Avrarmoglou, D. (2014). The pH in the Microenvironment of Human Mesenchymal Stem Cells Is a Critical Factor for Optimal Osteogenesis in Tissue-Engineered Constructs. *Tissue Engineering Part A*, 20(13–14), 1827–1840. <https://doi.org/10.1089/ten.tea.2013.0500>
 46. Xie, F., Wang, J., & Zhang, B. (2023). RefFinder: a web-based tool for comprehensively analyzing and identifying reference genes. *Functional & Integrative Genomics*, 23(2), 125. <https://doi.org/10.1007/s10142-023-01055-7>
 47. Kuo, Y.-H., Zaidi, S. K., Gornostaeva, S., Komori, T., Stein, G. S., & Castilla, L. H. (2009). Runx2 induces acute myeloid leukemia in cooperation with Cbfb-SMMHC in mice. *Blood*, 113(14), 3323–3332. <https://doi.org/10.1182/blood-2008-06-162248>
 48. Miron, R. J., Zohdi, H., Fujioka-Kobayashi, M., & Bosshardt, D. D. (2016). Giant cells around bone biomaterials: Osteoclasts or multinucleated giant cells? *Acta Biomaterialia*, 46, 15–28. <https://doi.org/10.1016/j.actbio.2016.09.029>
 49. Miron, R. J., & Bosshardt, D. D. (2018). Multinucleated Giant Cells: Good Guys or Bad Guys? *Tissue Engineering Part B: Reviews*, 24(1), 53–65. <https://doi.org/10.1089/ten.teb.2017.0242>
 50. Nerem, R. M. (2006). Tissue Engineering: The Hope, the Hype, and the Future. *Tissue Engineering*, 12(5), 1143–1150. <https://doi.org/10.1089/ten.2006.12.1143>
 51. Ashammakhi, N., GhavamiNejad, A., Tutar, R., Fricker, A., Roy, I., Chatzistavrou, X., ... Catterson, E. J. (2022). Highlights on Advancing Frontiers in Tissue Engineering. *Tissue Engineering Part B: Reviews*, 28(3), 633–664. <https://doi.org/10.1089/ten.teb.2021.0012>
 52. Chandra, P. K., Soker, S., & Atala, A. (2020). Tissue engineering: current status and future perspectives. In *Principles of Tissue Engineering* (pp. 1–35). Elsevier. <https://doi.org/10.1016/B978-0-12-818422-6.00004-6>
 53. Goshima, J., Goldberg, V. M., & Caplan, A. I. (1991). Osteogenic potential of culture-expanded rat marrow cells as assayed in vivo with porous calcium phosphate ceramic. *Biomaterials*, 12(2), 253–258.
 54. Mendes, S. C., Tibbe, J. M., Veenhof, M., Both, S., Oner, F. C., van Blitterswijk, C. A., & de Bruijn, J. D. (2004).

- Relation between in vitro and in vivo osteogenic potential of cultured human bone marrow stromal cells. *Journal of Materials Science: Materials in Medicine*, 15(10), 1123–1128. <https://doi.org/10.1023/B:JMSM.0000046394.53153.21>
55. Giannoni, P., Scaglione, S., Daga, A., Ilengo, C., Cilli, M., & Quarto, R. (2010). Short-Time Survival and Engraftment of Bone Marrow Stromal Cells in an Ectopic Model of Bone Regeneration. *Tissue Engineering Part A*, 16(2), 489–499. <https://doi.org/10.1089/ten.tea.2009.0041>
 56. Manassero, M., Paquet, J., Deschepper, M., Viateau, V., Retortillo, J., Bensidhoum, M., ... Petite, H. (2016). Comparison of Survival and Osteogenic Ability of Human Mesenchymal Stem Cells in Orthotopic and Ectopic Sites in Mice. *Tissue Engineering, Part A*, 22(5–6), 534–544. <https://doi.org/10.1089/ten.TEA.2015.0346>
 57. Ando, Y., Matsubara, K., Ishikawa, J., Fujio, M., Shohara, R., Hibi, H., ... Yamamoto, A. (2014). Stem cell-conditioned medium accelerates distraction osteogenesis through multiple regenerative mechanisms. *Bone*, 61, 82–90. <https://doi.org/10.1016/j.bone.2013.12.029>
 58. Osugi, M., Katagiri, W., Yoshimi, R., Inukai, T., Hibi, H., & Ueda, M. (2012). Conditioned Media from Mesenchymal Stem Cells Enhanced Bone Regeneration in Rat Calvarial Bone Defects. *Tissue Engineering Part A*, 18(13–14), 1479–1489. <https://doi.org/10.1089/ten.tea.2011.0325>
 59. Sims, N. A., Martin, T. J., & Quinn, J. M. W. (2016). Coupling: The Influences of Immune and Bone Cells. In *Osteoimmunology* (pp. 169–185). Elsevier. <https://doi.org/10.1016/B978-0-12-800571-2.00010-4>
 60. Chen, R., Hao, Z., Wang, Y., Zhu, H., Hu, Y., Chen, T. Li, J. (2022). Mesenchymal Stem Cell–Immune Cell Interaction and Related Modulations for Bone Tissue Engineering. *Stem Cells International*, 2022, 1–19. <https://doi.org/10.1155/2022/7153584>
 61. Budzynski, W., & Radzikowski, C. (1994). Cytotoxic Cs in Immunodeficient Athymic Mice. *Immunopharmacology and Immunotoxicology*, 16(3), 319–346. <https://doi.org/10.3109/08923979409007097>
 62. Salgado, A. J., Reis, R. L., Sousa, N., & M. Gimble, J. (2010). Adipose Tissue Derived Stem Cells Secretome: Soluble Factors and Their Roles in Regenerative Medicine. *Current Stem Cell Research & Therapy*, 5(2), 103–110. <https://doi.org/10.2174/157488810791268564>
 63. Wasnik, S., Rundle, C. H., Baylink, D. J., Yazdi, M. S., Carreon, E. E., Xu, Y., ... Tang, X. (2018). 1,25-Dihydroxyvitamin D suppresses M1 macrophages and promotes M2 differentiation at bone injury sites. *JCI Insight*, 3(17), e98773. <https://doi.org/10.1172/jci.insight.98773>
 64. Pajarinen, J., Lin, T., Gibon, E., Kohno, Y., Maruyama, M., Nathan, K., ... Goodman, S. B. (2019). Mesenchymal stem cell-macrophage crosstalk and bone healing. *Biomaterials*, 196, 80–89. <https://doi.org/10.1016/j.biomaterials.2017.12.025>
 65. Shin, R. L.-Y., Lee, C.-W., Shen, O. Y.-J., Xu, H., & Lee, O. K.-S. (2021). The Crosstalk between Mesenchymal Stem Cells and Macrophages in Bone Regeneration: A Systematic Review. *Stem Cells International*, 2021, 1–21. <https://doi.org/10.1155/2021/8835156>

To cite this article:

Manon Maroquenne#, Marianne Bourguignon#, Nathanael Laroquette # , Hanane El-Hafci , Morgane Margottin, Esther Potier and Delphine Logeart Avramoglou, # Co-first authors
The lower in vivo osteogenicity of adipose tissue-derived stem cells correlates with a higher innate immune response, *Stem Cell Reviews and Reports*, Published online: 29 August 2023,
DOI <https://doi.org/10.1007/s12015-023-10614-1>

Corresponding author:

Dr Delphine Logeart-Avramoglou, PhD

Laboratory of Bioengineering and Biomechanics for Bone and Articulariactions; UMR 7052, CNRS, Paris Diderot University, Sorbonne Paris-Cité, 10 avenue de Verdun 75010 Paris, France

Phone number: +33 1 57 27 85 63

E-mail: delphine.logeart@cnrs.fr

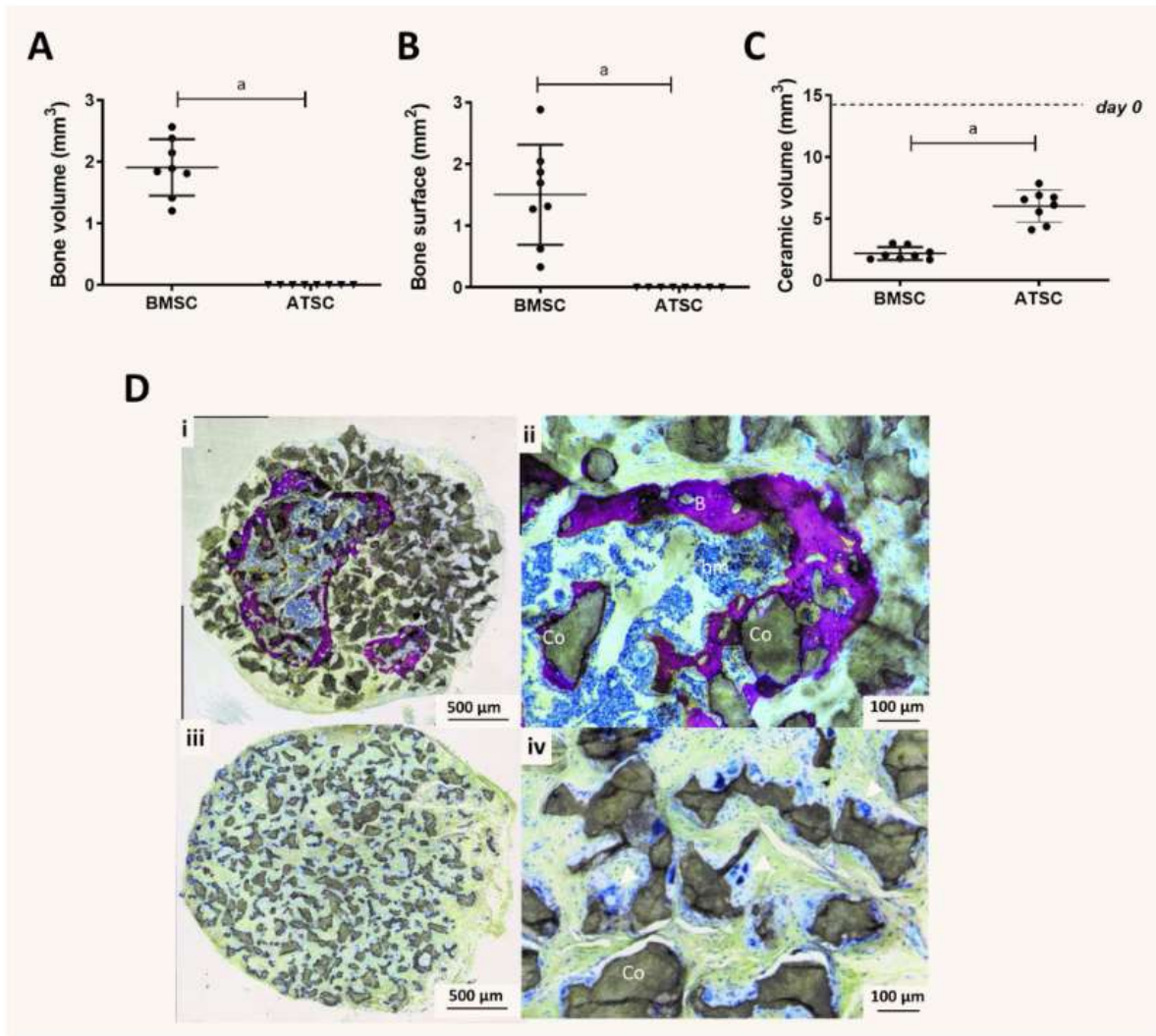


Figure 1: In vivo osteogenic potential of the implanted MSCs. The BMSCs or ATSCs were seeded on coral granules and implanted ectopically in nude mice for 8 weeks. (A) Quantification of the bone volume determined using μ -CT analysis. (B) Quantification of the bone surface determined using histomorphometry. (C) Quantification of the residual ceramic scaffold volume determined using μ -CT. Values are mean \pm SEM; n = 8. t-test: (a) p < 0.05. (D) Representative histology sections of either BMSC- (Di-Dii) or ATSC- (Diii-Div) containing constructs. Stain: Picrofuchsin and Stevenel's blue. Newly formed bone is evidenced in red (B); (Co) Coral granules; (bm) bone-marrow-like tissue; White arrow heads in Div frame point giant cells

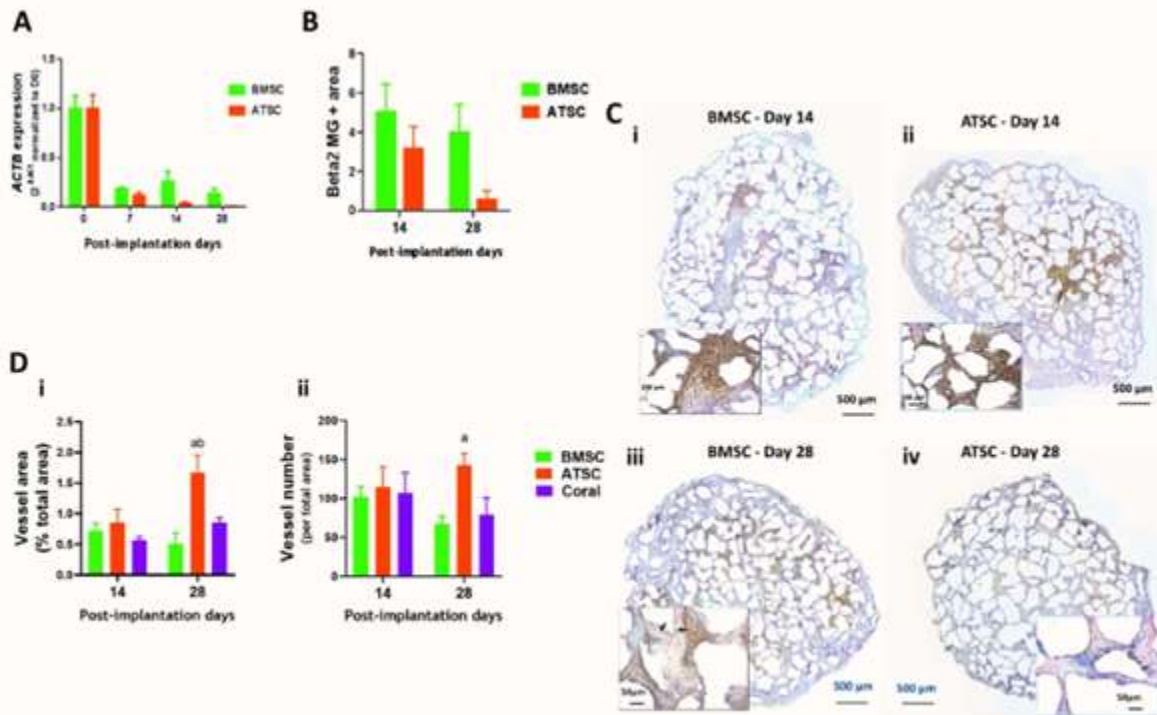


Figure 2: In vivo engraftment of human MSCs contained in the constructs. (A) Expression of the human ACTB gene normalized to 18S expression (expressed by both human and murine cells) in MSC-containing constructs excised on 0-, 7-, 14- and 28-days post-implantation. Values are mean \pm SEM. n = 6. (B-C) Implanted BMSC or ATSCs still present in the constructs explanted 14- and 28-days post-implantation were detected by immunostaining against human beta-2-microglobulin. (B) Quantification of human beta-2-microglobulin positive area per tissue section; Values are means \pm SEM. n=4. (C) Representative tissue sections of either BMSC- or ATSC-containing constructs immunostained against human beta-2-microglobulin. The black arrows point at positive labeled osteocytes. (D) Quantification of the surface area (i) and number (ii) of vessels on each section per tissue section stained with hematoxylin and eosin; Values are means \pm SEM. n=4. Two-way ANOVA with Tukey's post hoc test: (a) $p < 0.05$ versus results obtained from BMSC-containing constructs; (b) $p < 0.05$ versus results obtained from cell-free constructs (Coral group)

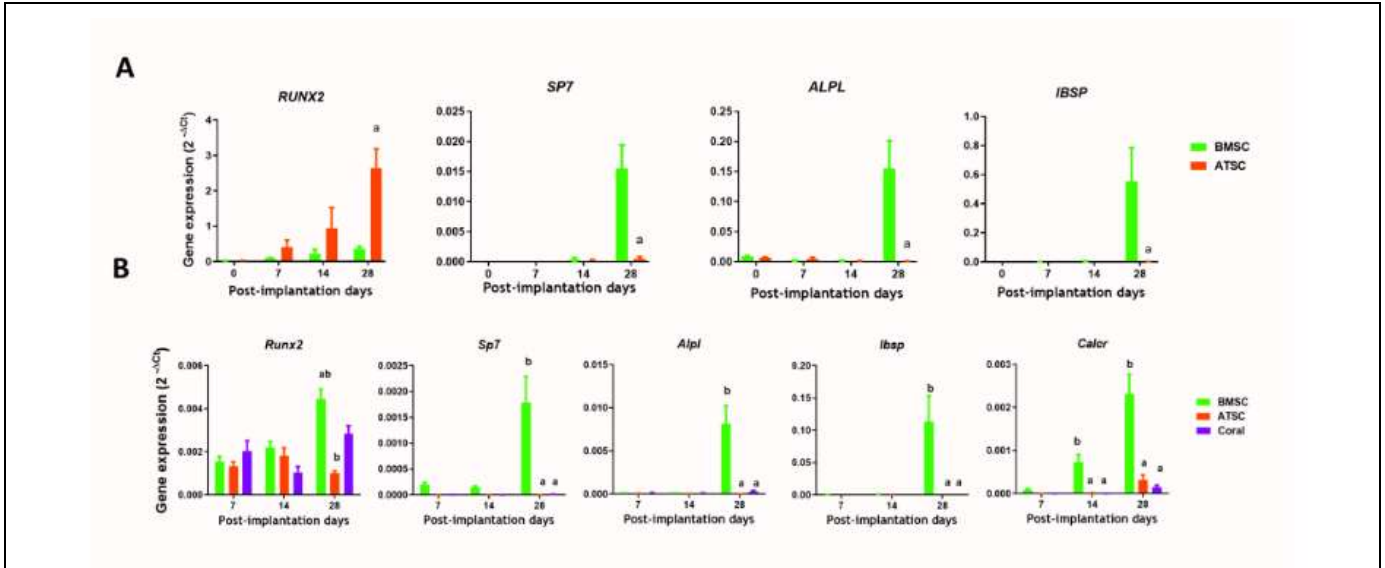
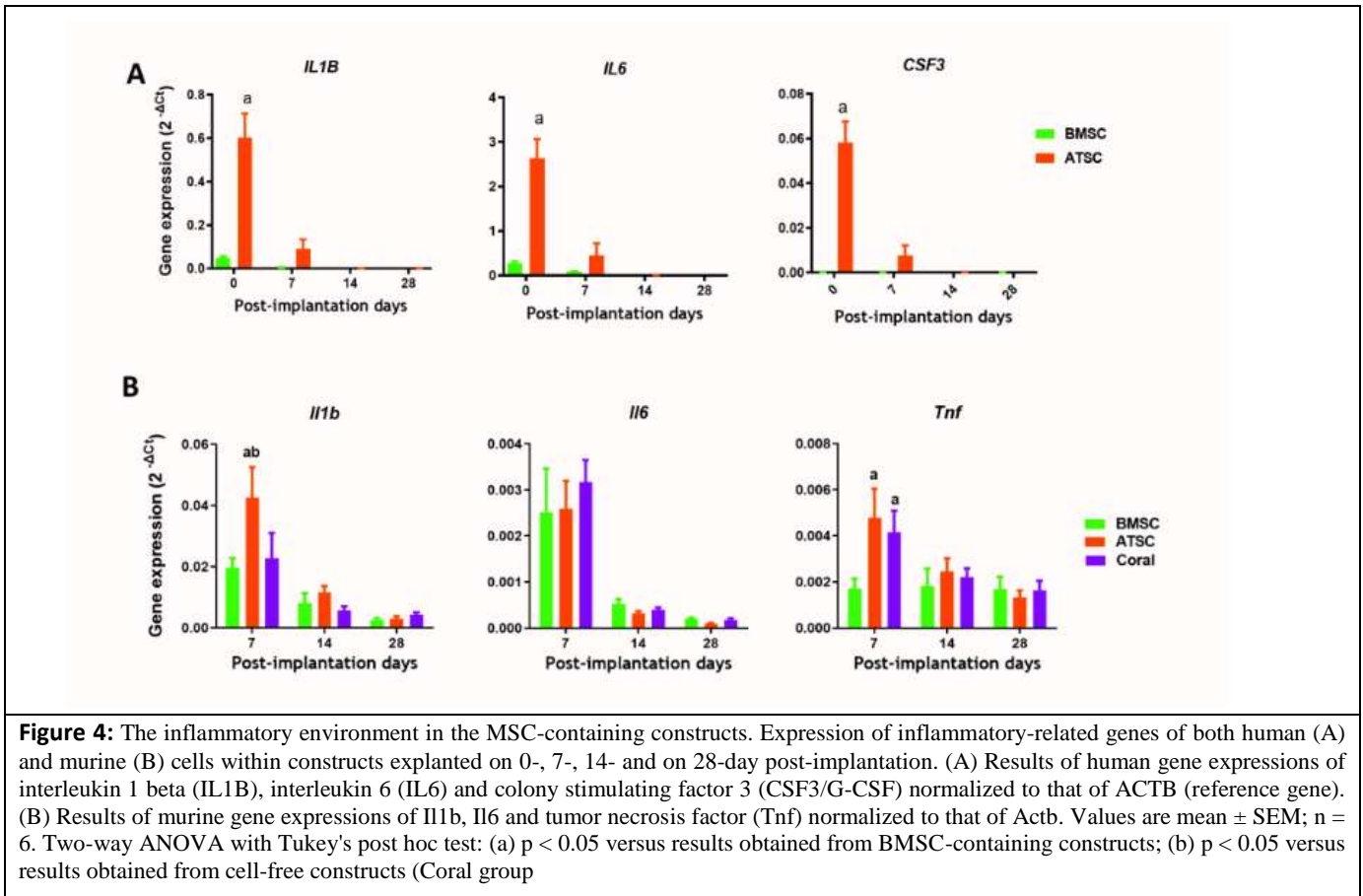


Figure 3: Osteogenic differentiation of both implanted MSCs and host recruited progenitors. Expression of osteogenesis-related genes of both (A) human and (B) murine cells within constructs excised on 0-, 7-, 14- and 28-day post-implantation. Results of respective human and murine gene expressions of RUNX family transcription factor 2 (RUNX2/Runx2), SP7 transcription factor/Osterix (SP7/Sp7), alkaline phosphatase (ALPL/Alpl), integrin-binding sialoprotein (IBSP/Ibsp) and murine calcitonin receptor (Calcr). Gene expressions were normalized to that of the respective human ACTB and murine Actb genes (reference gene). Values are mean ± SEM; n = 6. Two-way ANOVA with Tukey's post hoc test: (a) p < 0.05 versus results obtained from BMSC-containing constructs; (b) p < 0.05 versus results obtained from cell-free constructs (Coral group)



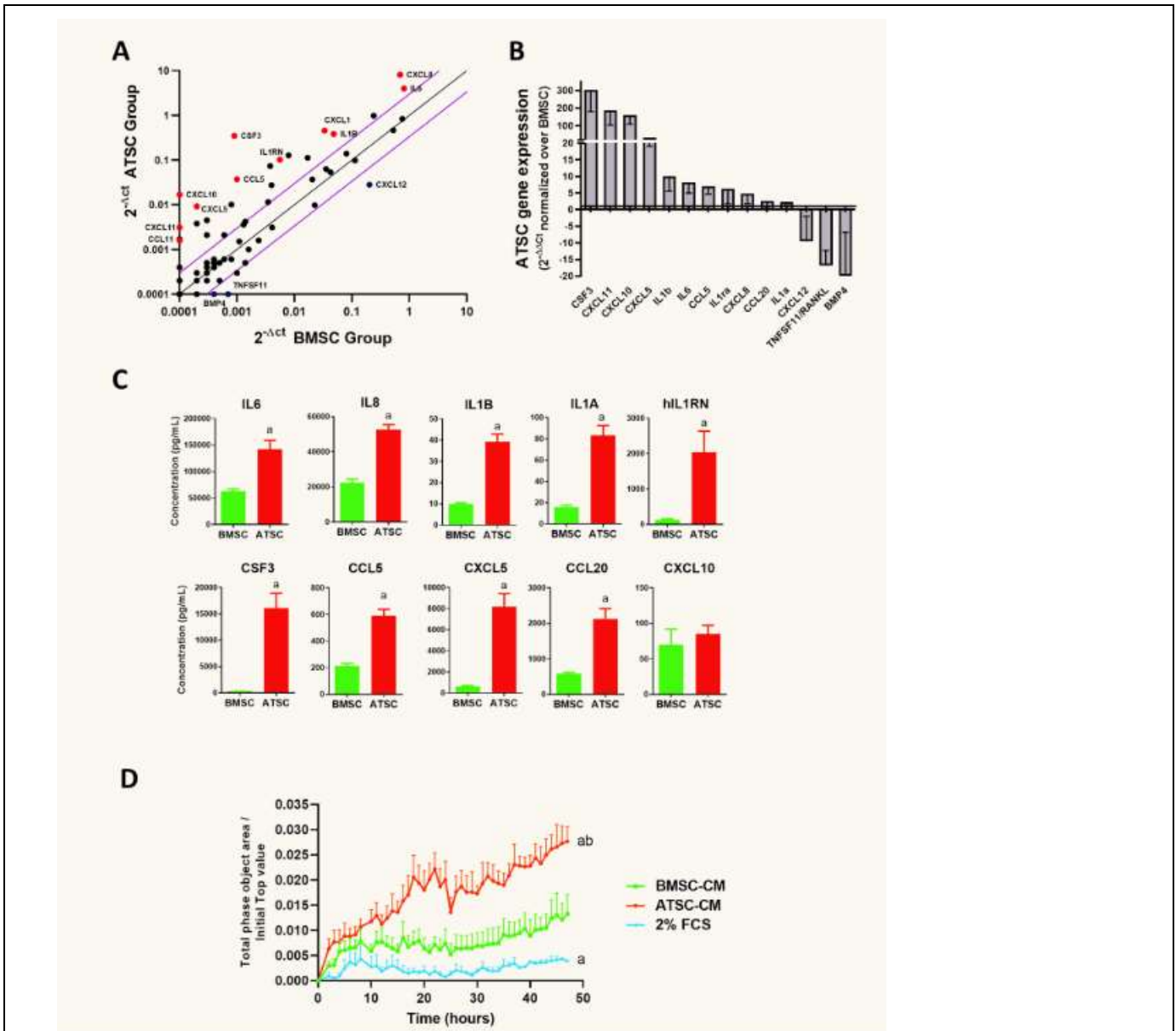


Figure 5: ATSCs are a source of inflammatory cytokines / chemokines that trigger macrophage attraction. (A) RT² Profiler PCR Array analysis of human cytokine and chemokine gene expression comparing the ATSCs and BMSCs contained in constructs at day 0 (before implantation). Data are represented as scatter plot on expression levels of the 84 genes tested. The dots represent expression for each gene using cDNA from n=6 replicates (that had been previously equally pooled) $\bar{}$. The black line (in the center) indicates unchanged gene levels; the boundaries (purple lines) represent the 3-fold regulation cut-off. The Red and Blue dots indicate upregulated and downregulated genes, respectively, which were further validated using Taqman hydrolysis probes. (B) Taqman validation of the genes identified using the RT Profiler array. The histogram represents fold-change of genes either up- or down-regulated construct-contained ATSCs compared to BMSCs. Values are mean \pm SEM for each replicate (n = 6). (C) Concentrations of cytokines released in the supernatants of construct-contained BMSCs and ATSCs cultured for 48 hours. Values are mean \pm SEM. n = 8. Mann-Whitney test: (a) p < 0.05 versus results obtained from BMSCs. (D) Results of macrophage chemotaxis induced by the contents in the supernatants of MSC-containing constructs. Monocytes were generated from PBMCs cultured in M-CSF for 6 days. Their real time migration was assessed using the IncuCyte device and the data represent the total area occupied by macrophages on the bottom well surface normalized by the top area occupied by cells at the beginning of the experiment (t = 0h). t = 0 hour. Values are mean \pm SEM. n = 4. Two-way ANOVA with Tukey's post hoc test: (a) p < 0.05 versus the results obtained using supernatant conditioned media from BMSC-containing constructs; (b) p < 0.05 versus results obtained using 2% fetal calf serum

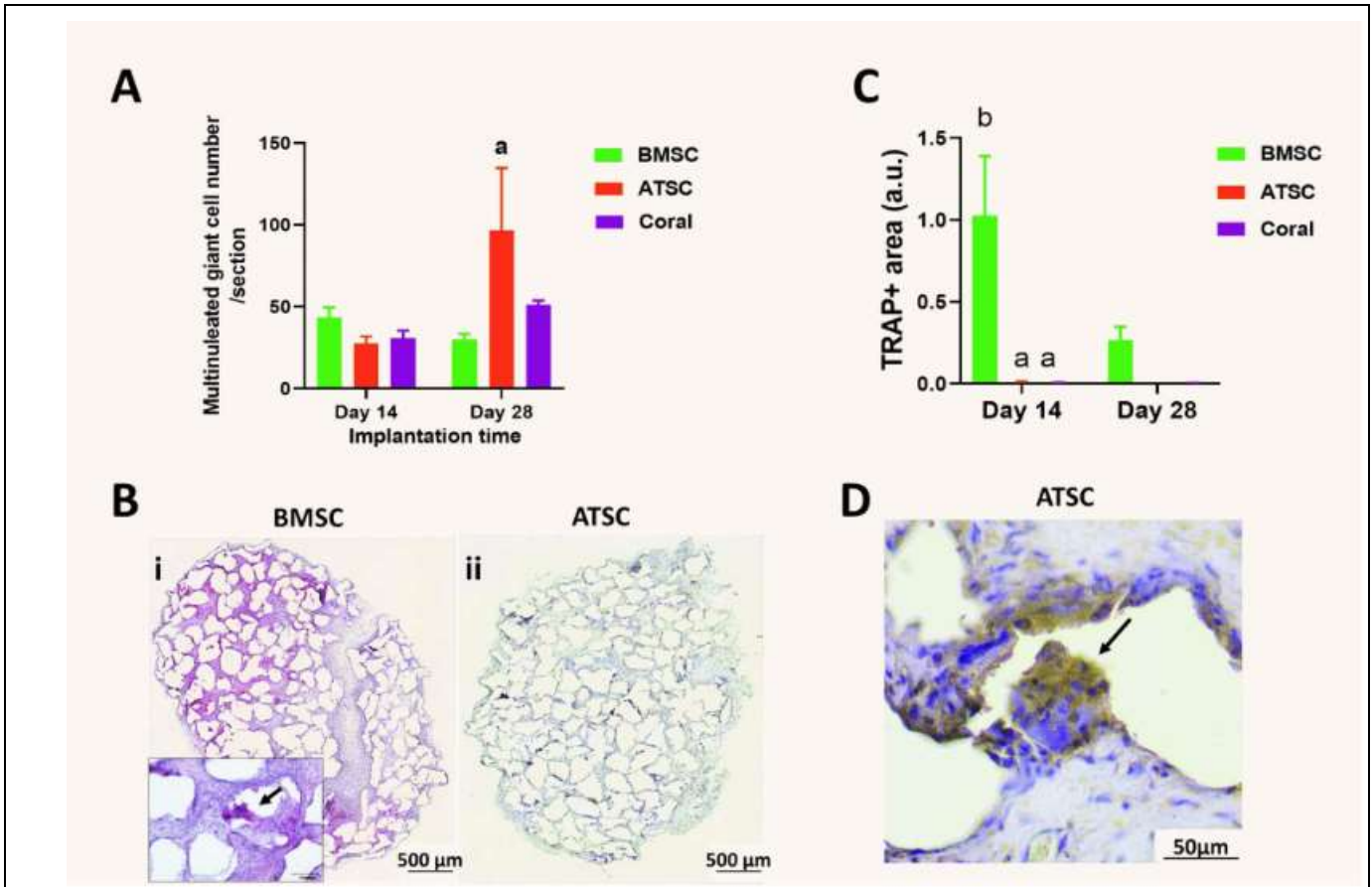


Figure 6: Osteoclasts were absent but multinuclear giant cells (MNGCs) were present in the ATSC-containing constructs. (A) Quantification of the multinucleated giant cells present per tissue section excised on days 14 and 28 post implantation; (n=4; three sections per construct were analyzed). (B) Representative TRAP-stained tissue sections from BMSC- (Bi) and ATSC- (Bii) containing constructs explanted 14 days post-implantation. Black arrow points a TRAP+ osteoclast. (C) Quantification of TRAP-positive area per tissue section; (n = 4). (D) Representative tissue sections from ATSC-containing constructs excised 28 days post-implantation immunostained against murine mannose receptor C type 1 (MRC1 / CD206, a MNGC marker). Black arrow points a MRC1 / CD206+ MNGC. Values are mean ± SEM. Two-way ANOVA with Tukey's post hoc test: (a) $p < 0.05$ versus results obtained from constructs containing BMSCs; (b) $p < 0.05$ versus results obtained from cell-free constructs (Coral group)

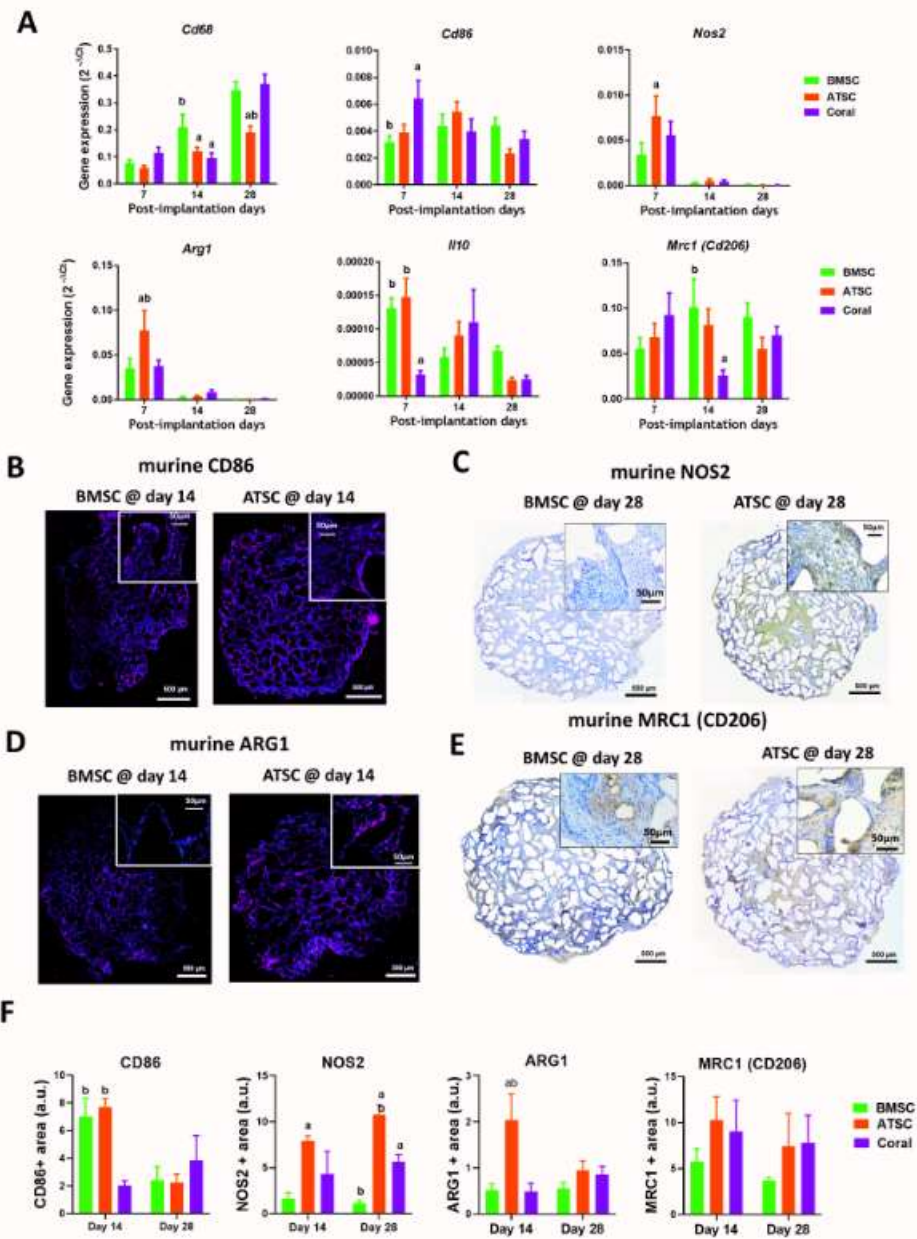


Figure 7: Macrophage recruitment within the MSC-containing constructs. (A) Expression of macrophage-related genes in constructs explanted on 7-, 14- and 28-days post-implantation. Results of murine gene expressions of the Cd68 (pan-macrophage marker), Cd86 and nitric oxide synthase 2 (Nos2) (M1 macrophage markers) and arginase 1 (Arg1), Il10 and Mrc1/Cd206 (M2 macrophage markers). These data were normalized to that of Actb (reference gene); n=6. (B-E) Representative immunostained tissue sections from cell constructs against the murine CD86 (Frame B) and NOS2 (Frame C) M1 markers, and against the murine ARG1 (Frame D) and MRC1 / CD206 (Frame E) M2 markers. (F) Quantifications of the CD86, NOS2, ARG1 and MRC1 / CD206 positive area per tissue section from constructs excised 14- and 28-days post-implantation; n = 4. Values are mean ± SEM. Two-way ANOVA with Tukey's post hoc test: (a) $p < 0.05$ versus results obtained from constructs containing BMSCs; (b) $p < 0.05$ versus results obtained from cell-free constructs (Coral group)

Human probes			
Gene symbol	Name	Alias symbols	Assay ID *
<i>ACTB</i>	actin beta	β -actin	Hs01060665_g1
<i>ALPL</i>	alkaline phosphatase biomineralization associated	HOPS; TNSALP; TNALP; TNAP	Hs01029144_m1
<i>BMP4</i>	bone morphogenetic protein 4	BMP2B	Hs03676628_s1
<i>CCL5</i>	C-C motif chemokine ligand 5	RANTES; SISd; TCP228; MGC17164	Hs00982282_m1
<i>CCL20</i>	C-C motif chemokine ligand 20	LARC; MIP-3a; exodus-1; ST38; CKb4	Hs00355476_m1
<i>CSF3</i>	colony stimulating factor 3	C17orf33; CSF3OS; GCSF	Hs99999083_m1
<i>CXCL5</i>	C-X-C motif chemokine ligand 5	ENA-78 ; SCYB5	Hs01099660_g1
<i>CXCL8</i>	C-X-C motif chemokine ligand 8	IL-8; SCYB8; LUCT; LECT; MDNCF; TSG-1; NAP-1; 3-10C; MONAP; AMCF-I; LYNAP; NAF; b-ENAP; GCP-1; K60; GCP1; NAP1	Hs00174103_m1
<i>CXCL10</i>	C-X-C motif chemokine ligand 10	C7; IFI10; INP10; IP-10; SCYB10; crg-2; gIP-10; mob-1	Hs01124251_g1
<i>CXCL11</i>	C-X-C motif chemokine ligand 11	H174; b-R1; I-TAC; IP-9	Hs00171138_m1
<i>CXCL12</i>	C-X-C motif chemokine ligand 2	GRO2; SCYB2; GROb; MIP-2a; MIP2; MIP2A; CINC-2a; MGSA-b	Hs00171022_m1
<i>IBSP</i>	integrin binding sialoprotein	BSP; SP-II; BSP-II	Hs00173720_m1
<i>IL1RN</i>	interleukin 1 receptor antagonist	IL1RA; ICIL-1RA; IL1F3; IRAP; IL-1RN; MGC10430	Hs00277299_m1
<i>IL1B</i>	interleukin 1 beta	IL1F2 ; IL-1B ; IL1-BETA	Hs01555410_m1
<i>IL6</i>	Interleukin 6	IFNB2; IL-6; BSF2; HGF; HSF	Hs00985639_m1
<i>RUNX2</i>	RUNX family transcription factor 2	CCD; CBFA1; CCD1; AML3; PEBP2A1	Hs01047973_m1
<i>SP7</i>	Sp7 transcription factor	osterix; OSX	Hs00541729_m1
<i>TNFSF11</i>	TNF superfamily member 11	TRANCE; RANKL; OPGL; ODF; CD254	Hs00243522_m1

Supplementary Table 1 : List of TaqMan Human Gene Expression Assays used in RT-PCR analysis

Murine probes			
Gene symbol	Name	Alternative names	Assay ID *
<i>Actb</i>	actin beta	Actx; beta-actin; E430023M04Rik	Mm01205647_g1
<i>Alpl</i>	alkaline phosphatase, biomineralization associated	Hops; Tnsalp; Tnalp; Tnap	Mm00475834_m1
<i>Angpt2</i>	angiopoietin 2	Ang2	Mm00545822_m1
<i>Arg1</i>	arginase 1	arginase, liver	Mm00475988_m1
<i>Calcr</i>	calcitonin receptor	Ctr, Ct-r	Mm00432282_m1
<i>Cd68</i>	CD68 molecule	Scard1; Gp110; Dkfzp686m18236; Lamp4	Mm03047343_m1
<i>Cd86</i>	CD86 molecule	B7.2; B7-2	Mm00444543_m1
<i>Ibsp</i>	integrin binding sialoprotein	Bsp; Sp-II; Bsp2; BspII	Mm00492555_m1
<i>Il1b</i>	interleukin 1 beta	Il1f2; Il-1b; Il1-beta	Mm00434228_m1
<i>Il10</i>	interleukin 10	Csif; Tgif; Il10a; Il-10	Mm00439614_m1
<i>Il6</i>	interleukin 6	Il-6	Mm00446190_m1
<i>Mrc1</i>	mannose receptor C type 1	Mrc111; Clec13d; Cd206; Ba541i19.1 Clec13dl	Mm00485148_m1
<i>Nos2</i>	nitric oxide synthase 2	Nos2a ; iNos ; Nos ; Hep-Nos	Mm00440502_m1
<i>Pecam1</i>	platelet and endothelial cell adhesion molecule 1	Cd31	Mm01242576_m1
<i>Runx2</i>	RUNX family transcription factor 2	Ccd; Cbfa1; Ccd1; Aml3; Pebp2a1	Mm00501580_m1
<i>Sp7</i>	Sp7 transcription factor	osterix; Osx	Mm00504574_m1
<i>Tnf</i>	tumor necrosis factor	Tnfa ; Tnfsf2; Dif; Tnf-alpha	Mm00443260_g1

Supplementary Table 1bis : List of TaqMan Murine Gene Expression Assays used in RT-PCR analysis

Supplementary Table 2: Minimum Information for Publication of Quantitative Real-Time PCR Experiments (MIQE) checklist

ITEM TO CHECK	Importance	Included ?	COMMENTS
EXPERIMENTAL DESIGN			
Definition of experimental and control groups	E	Y	see Materials and Methods section
Number within each group	E	Y	6 biological replicates (see Materials and Methods section)
Assay carried out by core lab or investigator's lab?	D	Y	Investigator's lab
Acknowledgement of authors' contributions	D	Y	Dissection/Homogenization/ RNA Extraction:NL. RT-qPCR: MM
SAMPLE			
Description	E	Y	see Materials and Methods section
Volume/mass of sample processed	D	NA	mix of ceramic granules and tissue
Microdissection or macrodissection	E	Y	macrodissection of constructs
Processing procedure	E	Y	see Materials and Methods section
If frozen - how and how quickly?	E	Y	snap-freezing of explanted constructs in nitrogen liquid and direct transfer at -80°C within minutes following animal euthanasia
If fixed - with what, how quickly?	E	NA	
Sample storage conditions and duration (especially for FFPE samples)	E	Y	stored at -80°C (max 1 month before being processed for RNA extraction)
NUCLEIC ACID EXTRACTION			
Procedure and/or instrumentation	E	Y	For all samples: Phenol-chloroform extraction (Trizol method) - Exact protocol available upon request For samples analyzed with RT ² profiler PCR array: additional purification using Rneasy mini kits
Name of kit and details of any modifications	E	Y	Trizol method
Source of additional reagents used	D	Y	Upon Request
Details of DNase or RNase treatment	E	N	no further DNase treatment was performed
Contamination assessment (DNA or RNA)	E	NA	all Taqman hydrolysis Probes span exons
Nucleic acid quantification	E	Y	Spectrophotometric analysis (at 280 nm and 260

			nm)
Instrument and method	E	Y	Molecular Devices SPECTRAMAX Plus with SpectraDrop 24 Kit
Purity (A260/A280)	D	Y	1.8 < Purity < 2.0
Yield	D	Y	
RNA integrity method/instrument	E	N	
RIN/RQI or Cq of 3' and 5' transcripts	E	N	
Electrophoresis traces	D	N	
Inhibition testing (Cq dilutions, spike or other)	E	N	
REVERSE TRANSCRIPTION			
Complete reaction conditions	E	Y	For each sample, 3 µg of the RNA was reversed-transcribed into cDNA using the Superscript II RT enzyme (Invitrogen) with oligo(dT) primers following the manufacture's recommendations
Amount of RNA and reaction volume	E	Y	3 µg of purified RNA in 20 µL reaction
Priming oligonucleotide (if using GSP) and concentration	E	Y	Random primers (Invitrogen) at 0.15 µg/µl vol reaction
Reverse transcriptase and concentration	E	Y	Superscript II RT enzyme (Invitrogen) at 10 U/µl vol reaction
Temperature and time	E	Y	10 min at 25°C / 50 min at 42°C / 15 min at 70°C
Manufacturer of reagents and catalogue numbers	D	Y	ref 18064014 / 18427013 / 48190011 (Invitrogen)
Cqs with and without RT	D*	N	
Storage conditions of cDNA	D	Y	-20°C
qPCR TARGET INFORMATION			
If multiplex, efficiency and LOD of each assay.	E	NA	
Sequence accession number	E	Y	Available; See https://www.thermofisher.com/fr/fr/home/life-science/pcr/real-time-pcr/real-time-pcr-assays.html
Location of amplicon	D	Y	Available; See https://www.thermofisher.com/fr/fr/home/life-science/pcr/real-time-pcr/real-time-pcr-assays.html
Amplicon length	E	Y	Available; See https://www.thermofisher.com/fr/fr/home/life-science/pcr/real-time-pcr/real-time-pcr-assays.html
<i>In silico</i> specificity screen (BLAST, etc)	E	Y	Available; See https://www.thermofisher.com/fr/fr/home/life-science/pcr/real-time-pcr/real-time-pcr-assays.html

			science/pcr/real-time-pcr/real-time-pcr-assays.html
Pseudogenes, retropseudogenes or other homologs?	D	Y	Available; See https://www.thermofisher.com/fr/fr/home/life-science/pcr/real-time-pcr/real-time-pcr-assays.html
Sequence alignment	D	Y	Available; See https://www.thermofisher.com/fr/fr/home/life-science/pcr/real-time-pcr/real-time-pcr-assays.html
Secondary structure analysis of amplicon	D	Y	Available; See https://www.thermofisher.com/fr/fr/home/life-science/pcr/real-time-pcr/real-time-pcr-assays.html
Location of each primer by exon or intron (if applicable)	E	Y	Available; See https://www.thermofisher.com/fr/fr/home/life-science/pcr/real-time-pcr/real-time-pcr-assays.html
What splice variants are targeted?	E	Y	Available; See https://www.thermofisher.com/fr/fr/home/life-science/pcr/real-time-pcr/real-time-pcr-assays.html
qPCR OLIGONUCLEOTIDES			
Primer sequences	E	NA	TaqMan™ Gene Expression Assay (FAM); see table 1 for assays IDs See https://www.thermofisher.com/fr/fr/home/life-science/pcr/real-time-pcr/real-time-pcr-assays.html
RTPrimerDB Identification Number	D	Y	Available; See https://www.thermofisher.com/fr/fr/home/life-science/pcr/real-time-pcr/real-time-pcr-assays.html
Probe sequences	D**	Y	Available; See https://www.thermofisher.com/fr/fr/home/life-science/pcr/real-time-pcr/real-time-pcr-assays.html
Location and identity of any modifications	E	Y	Available; See https://www.thermofisher.com/fr/fr/home/life-science/pcr/real-time-pcr/real-time-pcr-assays.html
Manufacturer of oligonucleotides	D	Y	Available; See https://www.thermofisher.com/fr/fr/home/life-science/pcr/real-time-pcr/real-time-pcr-assays.html
Purification method	D	Y	Available; See https://www.thermofisher.com/fr/fr/home/life-science/pcr/real-time-pcr/real-time-pcr-assays.html

			science/pcr/real-time-pcr/real-time-pcr-assays.html
qPCR PROTOCOL			
Complete reaction conditions	E	Y	
Reaction volume and amount of cDNA/DNA	E	Y	5 µL; 25 ng cDNA for mouse gene analysis and 75 ng for human gene analysis
Primer, (probe), Mg ⁺⁺ and dNTP concentrations	E	Y	1µl of TaqMan™ Gene Expression Assay (FAM) + 10 µl TaqMan™ Gene Expression Master Mix (4369510 Invitrogen)
Polymerase identity and concentration	E	Y	ADN polymérase AmpliTaq Gold in TaqMan™ Gene Expression Master Mix (4369510 Invitrogen)
Buffer/kit identity and manufacturer	E	Y	see kit TaqMan™ Gene Expression Master Mix (4369510 Invitrogen)
Exact chemical constitution of the buffer	D	Y	The manufacturer does not provide this information
Additives (SYBR Green I, DMSO, etc.)	E	Y	No additional additives
Manufacturer of plates/tubes and catalog number	D	Y	ThermoScientific; PCR plate ref AB-1400-L
Complete thermocycling parameters	E	Y	50°C 2min; 95°C 10min; 40x (95°C 15sec, 60°C 1min); END
Reaction setup (manual/robotic)	D	Y	manual
Manufacturer of qPCR instrument	E	Y	MyiQ™ Real-Time PCR Detection System (Biorad)
qPCR VALIDATION			
Evidence of optimisation (from gradients)	D	NA	
Specificity (gel, sequence, melt, or digest)	E	NA	Specificity guaranteed by the manufacturer of the TaqMan assays
For SYBR Green I, Cq of the NTC	E	NA	
Standard curves with slope and y-intercept	E	NA	
PCR efficiency calculated from slope	E	NA	optimized probes by Applied Biosystems ; see https://assets.thermofisher.com/TFS-Assets/LSG/Application-Notes/cms_040377.pdf
Confidence interval for PCR efficiency or standard error	D	NA	
r ² of standard curve	E	NA	
Linear dynamic range	E	NA	
Cq variation at lower limit	E	NA	
Confidence intervals throughout range	D	NA	
Evidence for limit of detection	E	Y	Cq < 37 for all reactions

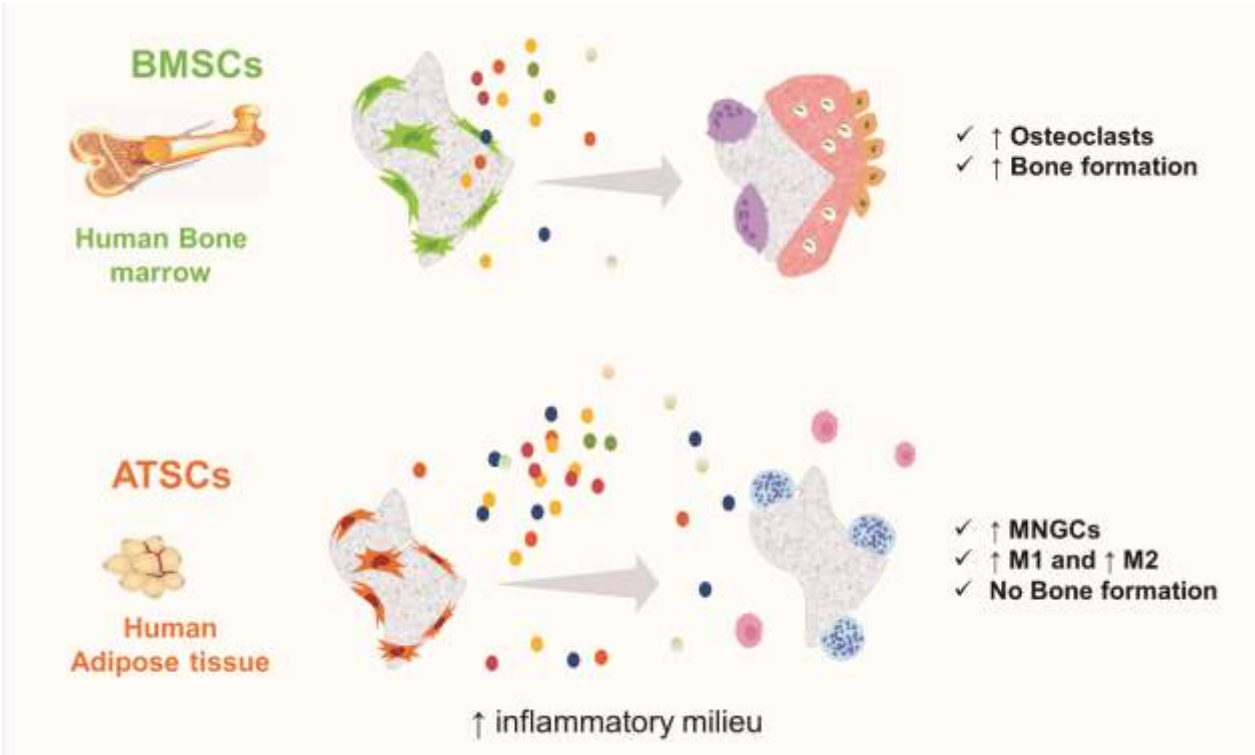
If multiplex, efficiency and LOD of each assay.	E	NA	
DATA ANALYSIS			
qPCR analysis program (source, version)	E	Y	MyiQ™ software (Biorad) version 1.0.410
Cq method determination	E	Y	auto Calculated
Outlier identification and disposition	E	Y	None of Cq values was discarded
Results of NTCs	E	Y	no amplification
Justification of number and choice of reference genes	E	Y	5 reference genes tested
Description of normalisation method	E	Y	Use of the web-based RefFinder tool (https://blooge.cn/RefFinder/) (geNorm, Normfinder, BestKeeper, and the comparative Δ -Ct method) to compare and rank the tested candidate reference genes
Number and concordance of biological replicates	D	Y	6 biological replicates
Number and stage (RT or qPCR) of technical replicates	E	Y	1 RT and 2 technical replicates for each biological replicate.
Repeatability (intra-assay variation)	E	Y	%CV \leq 3%
Reproducibility (inter-assay variation, %CV)	D	Y	%CV \leq 5%
Power analysis	D	N	
Statistical methods for result significance	E	Y	see Materials and Methods section
Software (source, version)	E	Y	GraphPad Prism, version 9.4.0; GraphPad Software, Inc
Cq or raw data submission using RDML	D	Y	Cq values upon request

Supplementary Table 2: Minimum Information for Publication of Quantitative Real-Time PCR Experiments (MIQE) checklist

Description	Gene name	Alias symbols	FC	log ₂ FC
<i>CSF3</i>	colony stimulating factor 3	<i>C17orf33</i> ; <i>CSF3OS</i> ; <i>GCSF</i>	376,37	8,6
<i>CXCL10</i>	C-X-C motif chemokine ligand 10	<i>C7</i> ; <i>IF110</i> ; <i>INP10</i> ; <i>IP-10</i> ; <i>SCYB10</i> ; <i>crg-2</i> ; <i>gIP-10</i> ; <i>mob-1</i>	167,27	7,4
<i>CXCL5</i>	C-X-C motif chemokine ligand 5	<i>ENA-78</i> ; <i>SCYB5</i>	60,38	5,9
<i>CCL5</i>	C-C motif chemokine ligand 5	<i>RANTES</i> ; <i>SISd</i> ; <i>TCP228</i> ; <i>MGC17164</i>	35,65	5,2
<i>CXCL11</i>	C-X-C motif chemokine ligand 11	<i>H174</i> ; <i>b-R1</i> ; <i>I-TAC</i> ; <i>IP-9</i>	30,61	4,9
<i>CCL20</i>	C-C motif chemokine ligand 20	<i>LARC</i> ; <i>MIP-3a</i> ; <i>exodus-1</i> ; <i>ST38</i> ; <i>CKb4</i>	19,24	4,3
<i>IL1RN</i>	interleukin 1 receptor antagonist	<i>IL1RA</i> ; <i>ICIL-1RA</i> ; <i>IL1F3</i> ; <i>IRAP</i> ; <i>IL-1RN</i> ; <i>MGC10430</i>	18,20	4,2
<i>CCL17</i>	C-C motif chemokine ligand 17	<i>SCYA17</i> ; <i>TARC</i> ; <i>ABCD-2</i>	17,10	4,1
<i>IL11</i>	interleukin 11	<i>AGIF</i> ; <i>IL-11</i>	16,07	4,0
<i>CCL3</i>	C-C motif chemokine ligand 3	<i>SCYA3</i> ; <i>G0S19-1</i> ; <i>LD78ALPHA</i> ; <i>MIP-1-alpha</i>	16,07	4,0
<i>CCL11</i>	C-C motif chemokine ligand 11	<i>SCYA11</i> ; <i>eotaxin-1</i> ; <i>MGC22554</i>	15,52	4,0
<i>TNFSF13B</i>	TNF superfamily member 13b	<i>TNFSF20</i> ; <i>BAFF</i> ; <i>THANK</i> ; <i>BLYS</i> ; <i>TALL1</i> ; <i>CD257</i>	13,99	3,8
<i>CXCL1</i>	C-X-C motif chemokine ligand 1	<i>MGSA</i> ; <i>GRO1</i> ; <i>FSP</i> ; <i>SCYB1</i> ; <i>GROa</i> ; <i>MGSA-a</i> ; <i>NAP-3</i>	13,70	3,8
<i>IL23A</i>	interleukin 23 subunit alpha	<i>SGRF</i> ; <i>IL23P19</i> ; <i>IL-23</i> ; <i>IL-23A</i> ; <i>P19</i>	13,51	3,8
<i>CXCL8</i>	C-X-C motif chemokine ligand 8	<i>IL-8</i> ; <i>SCYB8</i> ; <i>LUCT</i> ; <i>LECT</i> ; <i>MDNCF</i> ; <i>TSG-1</i> ; <i>NAP-1</i> ; <i>3-10C</i> ; <i>MONAP</i> ; <i>AMCF-1</i> ; <i>LYNAP</i> ; <i>NAF</i> ; <i>b-ENAP</i> ; <i>GCP-1</i> ; <i>K60</i> ; <i>GCPI1</i> ; <i>NAP1</i>	11,68	3,5
<i>IL1B</i>	interleukin 1 beta	<i>IL1F2</i> ; <i>IL-1B</i> ; <i>IL1-BETA</i>	7,92	3,0
<i>CCL7</i>	C-C motif chemokine ligand 7	<i>SCYA6</i> ; <i>SCYA7</i> ; <i>NC28</i> ; <i>FIC</i> ; <i>MARC</i> ; <i>MCP3</i>	7,55	2,9
<i>BMP6</i>	bone morphogenetic protein 6	<i>VGR</i> ; <i>VGR1</i>	6,90	2,8
<i>IL1A</i>	interleukin 1 alpha	<i>IL-1A</i> ; <i>IL1</i> ; <i>IL1-ALPHA</i> ; <i>IL1F1</i>	6,62	2,7
<i>IL6</i>	Interleukin 6	<i>IFNB2</i> ; <i>IL-6</i> ; <i>BSF2</i> ; <i>HGF</i> ; <i>HSF</i>	4,98	2,3
<i>CXCL2</i>	C-X-C motif chemokine ligand 2	<i>GRO2</i> ; <i>SCYB2</i> ; <i>GROb</i> ; <i>MIP-2a</i> ; <i>MIP2</i> ; <i>MIP2A</i> ; <i>CINC-2a</i> ; <i>MGSA-b</i>	4,07	2,0
<i>CXCL9</i>	C-X-C motif chemokine ligand 9	<i>CMK</i> ; <i>MIG</i> ; <i>Humig</i> ; <i>SCYB9</i> ; <i>crg-10</i>	3,83	1,9
<i>TNF</i>	tumor necrosis factor	<i>TNFA</i> ; <i>TNFSF2</i> ; <i>DIF</i> ; <i>TNF-alpha</i>	3,40	1,8
<i>CSF2</i>	colony stimulating factor 2	<i>GM-CSF</i>	3,24	1,7
<i>TNFSF10</i>	TNF superfamily member 10	<i>TRAIL</i> ; <i>Apo-2L</i> ; <i>CD253</i> ; <i>TL2</i> ; <i>TANCR</i>	3,00	1,6
<i>IL24</i>	interleukin 24	<i>C49A</i> ; <i>FISP</i> ; <i>IL10B</i> ; <i>MDA7</i> ; <i>MOB5</i>	2,74	1,5
<i>CCL13</i>	C-C motif chemokine ligand 13	<i>SCYA13</i> ; <i>MCP-4</i> ; <i>NCC-1</i> ; <i>SCYL1</i> ; <i>CKb10</i> ; <i>MGC17134</i>	2,37	1,2
<i>CCL2</i>	C-C motif chemokine ligand 2	<i>SCYA2</i> ; <i>MCP1</i> ; <i>MCP-1</i> ; <i>MCAF</i> ; <i>SMC-CF</i> ; <i>GDCF-2</i> ; <i>HC11</i> ; <i>MGC9434</i>	1,81	0,9
<i>TNFRSF11B</i>	TNF receptor superfamily member 11b	<i>OCIF</i> ; <i>OPG</i> ; <i>TR1</i>	1,76	0,8
<i>LIF</i>	LIF interleukin 6 family cytokine	<i>CDF</i> ; <i>DIA</i> ; <i>HILDA</i>	1,72	0,8
<i>IL22</i>	interleukin 22	<i>ILTIF</i> ; <i>IL-21</i> ; <i>zcyto18</i> ; <i>IL-TIF</i> ; <i>IL-D110</i> ; <i>TIFa</i> ; <i>TIFIL-23</i> ; <i>IL-22</i> ; <i>MGC79382</i> ; <i>MGC79384</i>	1,46	0,5
<i>IL21</i>	interleukin 21	<i>IL-21</i> ; <i>Za11</i>	1,43	0,5
<i>IL27</i>	interleukin 27	<i>IL30</i> ; <i>IL-27</i> ; <i>p28</i> ; <i>IL27p28</i> ; <i>IL-27A</i> ; <i>IL27A</i> ; <i>MGC71873</i>	1,39	0,5
<i>IL7</i>	interleukin 7	<i>IL-7</i>	1,32	0,4
<i>CSF1</i>	colony stimulating factor 1	<i>CSF-1</i> ; <i>M-CSF</i> ; <i>MGC31930</i>	1,25	0,3
<i>LTB</i>	lymphotoxin beta	<i>TNFC</i> ; <i>TNFSF3</i> ; <i>p33</i>	1,24	0,3
<i>IL13</i>	interleukin 13	<i>P600</i> ; <i>IL-13</i> ; <i>ALRH</i> ; <i>BHR1</i> ; <i>MGC116786</i> ; <i>MGC116788</i> ; <i>MGC116789</i>	1,24	0,3
<i>NODAL</i>	nodal growth differentiation factor		1,15	0,2

<i>IL18</i>	interleukin 18	<i>IGIF ; IL-18 ; IL-1g ; IL1F4</i>	1,13	0,2
<i>IL16</i>	interleukin 16	<i>LCF; IL-16; prIL-16; HsT19289; FLJ42735; FLJ16806</i>	1,11	0,2
<i>MIF</i>	macrophage migration inhibitory factor	<i>GIF; GLIF</i>	1,10	0,1
<i>CCL1</i>	C-C motif chemokine ligand 1	<i>I-309; P500; SCYA1; SISE; TCA3</i>	1,09	0,1
<i>LTA</i>	lymphotoxin alpha	<i>LT; TNFB; TNFSF1</i>	1,05	0,1
<i>CNTF</i>	ciliary neurotrophic factor	<i>HCNTF</i>	-1,00	0,0
<i>CD40LG</i>	CD40 ligand	<i>HIGM1; IMD3; TNFSF5; CD40L; TRAP; gp39; hCD40L; CD154; CD40-L; HIGM1; T-BAM</i>	-1,04	-0,1
<i>THPO</i>	thrombopoietin	<i>MGDF; TPO; MPLLG</i>	-1,05	-0,1
<i>VEGFA</i>	vascular endothelial growth factor A	<i>VEGF; VPF</i>	-1,13	-0,2
<i>IL17F</i>	interleukin 17F	<i>IL-17F/ML-1/ML1</i>	-1,14	-0,2
<i>GPI</i>	glucose-6-phosphate isomerase	<i>AMF ; NLK</i>	-1,15	-0,2
<i>SPP1</i>	secreted phosphoprotein 1	<i>BNSP; OPN; BSPI; ETA-1; lnc-PKD2-2-3</i>	-1,29	-0,4
<i>BMP2</i>	bone morphogenetic protein 2	<i>BMP2A</i>	-1,30	-0,4
<i>IL3</i>	interleukin 3	<i>IL-3; MULTI-CSF; MCGF; MGC79398; MGC79399</i>	-1,39	-0,5
<i>CX3CL1</i>	C-X3-C motif chemokine ligand 1	<i>SCYD1; NTN; C3Xkine; ABCD-3; CX3C3; CXC3</i>	-1,51	-0,6
<i>IL12A</i>	interleukin 12A	<i>NKSF1; CLMF; IL-12; NFSK; P35</i>	-1,65	-0,7
<i>IL4</i>	interleukin 4	<i>BSF1; IL-4; BCGF1; BCGF-1; MGC79402</i>	-1,66	-0,7
<i>TGFB2</i>	transforming growth factor beta 2		-2,30	-1,2
<i>MSTN</i>	myostatin	<i>GDF8</i>	-2,72	-1,4
<i>CXCL16</i>	C-X-C motif chemokine ligand 16	<i>SR-PSOX; CXCLG16; SRPSOX</i>	-2,90	-1,5
<i>C5</i>	complement C5	<i>CPAMD4; C5a; C5b</i>	-3,28	-1,7
<i>BMP4</i>	bone morphogenetic protein 4	<i>BMP2B</i>	-3,74	-1,9
<i>TNFSF11</i>	TNF superfamily member 11	<i>TRANCE; RANKL; OPGL; ODF; CD254</i>	-6,47	-2,7
<i>CXCL12</i>	C-X-C motif chemokine ligand 12	<i>SDF1A; SDF1B; SDF1; SCYB12; PBSF; TLSF-a; TLSF-b; TPARI</i>	-7,23	-2,9

Supplementary Table 3: Cytokine / Chemokine -related genes differentially expressed in ATSCs versus BMSCs contained in the constructs using the RT²-PCR array. **FC:** Fold change in ATSCs versus BMSCs



Supplementary Figure: graphical abstract